

Longboard with Automatic Braking

Raymond Hoyle, Project Manager  
Logan Mashchak, Software Manager  
Corey Miller, Hardware Manager  
Ben Roter, Archivist

Department of Electrical and Computer Engineering

**Honors Research Project**

Submitted to

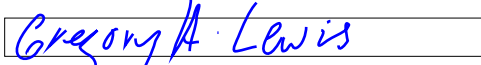
*The Williams Honors College  
The University of Akron*

Approved:




Date: 

Honors Project Sponsor (signed)



Honors Project Sponsor (printed)




Date: 

Reader (signed)



Reader (printed)



Date: 


Reader (signed)



Reader (printed)

Accepted:



Date: 

Honors Department Advisor (signed)



Honors Department Advisor (printed)



Date: 

Department Chair (signed)



Department Chair (printed)

Longboard with Automatic Braking

Raymond Hoyle, Project Manager  
Logan Mashchak, Software Manager  
Corey Miller, Hardware Manager  
Ben Roter, Archivist

Department of Electrical and Computer Engineering

**Honors Research Project**

Submitted to

*The Williams Honors College  
The University of Akron*

Approved:

[Signature box]

Date: [Date box]

Honors Project Sponsor (signed)

[Signature box]

Honors Project Sponsor (printed)

*Nathan Ida*

Date: *4/5/2021*

Reader (signed)

*NATHAN IDA*

Reader (printed)

[Signature box]

Date: [Date box]

Reader (signed)

[Signature box]

Reader (printed)

Accepted:

[Signature box]

Date: [Date box]

Honors Department Advisor (signed)

[Signature box]

Honors Department Advisor (printed)

[Signature box]

Date: [Date box]

Department Chair (signed)

[Signature box]

Department Chair (printed)

## **Honors Summary**

Ben Roter was responsible for designing the charge controller, voltage regulation, and Hall effect sensor hardware subsystems for the longboard anti-lock braking system (ABS) outlined in the design report. He researched different battery types and battery charging methods, different types of voltage regulators so that all the control system electronics would function properly, and different types of sensors and materials used for measuring wheel speeds. The devices and methods chosen for the subsystems mentioned above were successful when demonstrating them for the longboard ABS application. Further testing needs to be done so that the above hardware subsystems interface properly with the other hardware and software blocks of the ABS design, and further decisions need to be made about how best to mount both the Hall effect sensors and the rest of the electronics to the bottom of the longboard.

Logan Mashchak was responsible for designing the braking logic software algorithm for determining if the longboard exceeds 12 mph so that if that condition is met, the brakes could be applied. Additionally, he developed the slip conditional software algorithm outlined in the design report for determining if slip is occurring, as well as the software responsible for pulse width modulation (PWM) communication to the braking unit. He also assisted in the development of the complementary filter for the inertial measurement unit (IMU) in order to determine the angle of the board, as well as the calculation and unit conversion software for measuring wheel speed. Further integration and testing need to be done so that these algorithms interface with the other hardware and software subsystems properly while remaining within the bounds of the ABS system response time outlined in the design report.

## **Abstract**

The automatic longboard anti-lock braking system is a system designed to prevent a longboard from exceeding 12 mph while considering slipping and skidding, making it safer to ride a longboard. Speed limiting will be accomplished through wheel speed and incline angle measurements and brakes engaging or disengaging depending on internal decisions. Excess energy will be removed from the ABS as heat. Wheel speed and incline angle testing were done with a wheel speed sensor and an inertial measurement unit, respectively. Internal decisions were tested with programming a microcontroller, and braking was tested with motors. The wheel speed sensor yielded measurements within 2% of corresponding tachometer measurements, with the sensor and tachometer measuring 1304 rpm and 1281 rpm in one instance, respectively. The IMU gave results within 5% of the actual incline values, and the microcontroller correctly responded to input speed scenarios. The motors generated 2.205 V at 13 mA when unloaded and dropped to 1.900 V and 1.241 V when directly connected and when loaded with 500 m $\Omega$  of resistance. From these results, it was determined that the design would be feasible for physical implementation.

# Longboard with Automatic Braking

## Project Design Report

Team 11

Raymond Hoyle, Project Manager

Logan Mashchak, Software Manager

Corey Miller, Hardware Manager

Ben Roter, Archivist

Faculty Advisor: Dr. Robert Veillette

Date Submitted: 04/09/2021

# Table of Contents

<b>List of Figures</b> .....	iii
<b>List of Tables</b> .....	iv
<b>Abstract (RH, LM, CM, BR)</b> .....	1
<b>1. Problem Statement</b> .....	1
<b>1.1. Need (RH)</b> .....	1
<b>1.2. Objective (BR)</b> .....	2
<b>1.3. Background (RH, LM, CM, BR)</b> .....	2
<b>1.4. Marketing Requirements (RH)</b> .....	7
<b>2. Engineering Analysis</b> .....	7
<b>2.1. Batteries (BR)</b> .....	7
<b>2.2. Electronics</b> .....	10
<b>2.2.1. Charge Management (BR)</b> .....	10
<b>2.2.2. Voltage Regulation (BR)</b> .....	13
<b>2.3. Sensors</b> .....	14
<b>2.3.1. Wheel Velocity Measurement (BR)</b> .....	14
<b>2.3.2. Angle of Elevation Measurement (CM)</b> .....	19
<b>2.4. Communications (CM)</b> .....	21
<b>2.5. Electromechanics (RH)</b> .....	23
<b>2.6. Embedded Systems (LM)</b> .....	25
<b>3. Engineering Requirements Specification (RH, LM, CM, BR)</b> .....	27
<b>4. Engineering Standards Specification</b> .....	28
<b>4.1. Safety (LM)</b> .....	28
<b>4.2. Data Formats (CM)</b> .....	31
<b>4.3. Programming Languages (LM)</b> .....	31

<b>5. Accepted Technical Design</b> .....	32
<b>5.1. Hardware Design</b> (RH, LM, CM, BR) .....	32
<b>5.1.1. Level 0</b> .....	32
<b>5.1.2. Level 1</b> .....	33
<b>5.1.3. Level 2</b> .....	35
<b>5.1.4. Hardware Schematics</b> .....	38
<b>5.2. Software Design</b> (LM, CM) .....	46
<b>5.2.1. Level 0</b> .....	46
<b>5.2.2. Level 1</b> .....	47
<b>5.2.3. Level 2</b> .....	48
<b>5.2.4. Software Pseudocode, Flow Charts, and Formal Code</b> .....	50
<b>6. Mechanical Sketch</b> (LM) .....	60
<b>7. Team Information</b> (RH, LM, CM, BR) .....	60
<b>8. Parts List</b> (RH, LM, CM, BR) .....	61
<b>8.1. Part List</b> .....	61
<b>8.2. Materials Budget List</b> .....	62
<b>9. Project Schedules</b> (RH, LM, CM, BR) .....	63
<b>10. Conclusions and Recommendations</b> (RH, LM, CM, BR) .....	64
<b>11. References</b> (RH, LM, CM, BR) .....	66
<b>12. Datasheets</b> (RH, LM, CM, BR) .....	68

## List of Figures

<b>Figure 1:</b> Magnetic Flux Densities v. Axial Distance .....	17
<b>Figure 2:</b> Sensor Waveform .....	19
<b>Figure 3:</b> Free Body Diagram of a System Consisting of Two Rigid Bodies .....	29
<b>Figure 4:</b> Level 0 Hardware Block Diagram .....	32
<b>Figure 5:</b> Level 1 Hardware Block Diagram .....	34
<b>Figure 6:</b> Level 2 Hardware Block Diagram .....	35
<b>Figure 7:</b> Charge Controller Circuit Schematic .....	38
<b>Figure 8:</b> Longboard Control System Schematic .....	41
<b>Figure 9:</b> Level 0 Software Block Diagram .....	46
<b>Figure 10:</b> Level 1 Software Block Diagram .....	47
<b>Figure 11:</b> Level 2 Software Block Diagram .....	48
<b>Figure 12:</b> Velocity Calculation Pseudocode .....	51
<b>Figure 13:</b> Velocity Calculation Flow Chart .....	51
<b>Figure 14:</b> Formal Velocity Calculation Code .....	52
<b>Figure 15:</b> Pseudocode of IMU Readings and Calculations .....	54
<b>Figure 16:</b> Flow Chart of IMU Readings .....	54
<b>Figure 17:</b> Formal Code for Reading Gyroscope .....	55
<b>Figure 18:</b> Formal Code for Reading Accelerometer .....	55
<b>Figure 19:</b> Formal Complementary Filter Code .....	56
<b>Figure 20:</b> Pseudocode for Braking Conditionals .....	57
<b>Figure 21:</b> Flow Chart for Braking Conditionals .....	58
<b>Figure 22:</b> Formal Braking Conditionals Code .....	59
<b>Figure 23:</b> Longboard Control System Mechanical Sketch .....	60
<b>Figure 24:</b> Parts List .....	61
<b>Figure 25:</b> Materials Budget List .....	62
<b>Figure 26:</b> Midterm Gantt Chart .....	63
<b>Figure 27:</b> Final Gantt Chart .....	64



## List of Tables

<b>Table 1:</b> Marketing Requirements .....	7
<b>Table 2:</b> Engineering Requirements with Marketing Requirements and Justification .....	27
<b>Table 3:</b> Level 0 Hardware Functional Requirement Table .....	33
<b>Table 4:</b> Level 1 Hardware Function Requirement Tables .....	34
<b>Table 5:</b> Level 2 Hardware Function Requirement Tables .....	36
<b>Table 6:</b> Level 0 Software Functional Requirement Table .....	46
<b>Table 7:</b> Level 1 Software Functional Requirement Tables .....	47
<b>Table 8:</b> Level 2 Software Functional Requirement Tables .....	48

## **Abstract (RH, LM, CM, BR)**

The automatic longboard anti-lock braking system is a system designed to prevent a longboard from exceeding 12 mph while considering slipping and skidding, making it safer to ride a longboard. Speed limiting will be accomplished through wheel speed and incline angle measurements and brakes engaging or disengaging depending on internal decisions. Excess energy will be removed from the ABS as heat. Wheel speed and incline angle testing were done with a wheel speed sensor and an inertial measurement unit, respectively. Internal decisions were tested with programming a microcontroller, and braking was tested with motors. The wheel speed sensor yielded measurements within 2% of corresponding tachometer measurements, with the sensor and tachometer measuring 1304 rpm and 1281 rpm in one instance, respectively. The IMU gave results within 5% of the actual incline values, and the microcontroller correctly responded to input speed scenarios. The motors generated 2.205 V at 13 mA when unloaded and dropped to 1.900 V and 1.241 V when directly connected and when loaded with 500 m $\Omega$  of resistance. From these results, it was determined that the design would be feasible for physical implementation.

## **1. Problem Statement**

### **1.1. Need (RH)**

According to the Center for Disease Control and Prevention (CDC), between 2011 and 2014, approximately 8.6 million injuries involving sports and recreational activities were reported in the United States (34.1 injuries per 1000 people when applying an age-adjusted rate), 64.9% of which involved people between the ages of 5 and 24. With respect to skateboarding,

according to the *Injury Epidemiology* journal, as of 2008, at least 64.5 thousand children and teens between the ages of 5 and 19, were admitted to emergency rooms due to injuries per year. Due to these underlying factors, it would be extremely beneficial for there to be an electric skateboard or longboard that utilizes a system to manage speed.

## **1.2. Objective (BR)**

The shortcoming of safety features on classic skateboards can be mitigated with a new design. The goal is to add an automatic braking feature to help prevent injuries while riding at high speeds. Automatic skateboard braking will be realized with the integration of tachometers, accelerometers, brake control systems, and a host processor. The host processor will be used to interpret the data from the sensors. Decisions to activate the brakes will be made when the sensor data indicates the skateboard is traveling at unsafe speeds.

## **1.3. Background (BR, LM, CM, RH)**

Everything is all fun and games until somebody gets hurt. No matter how many times parents tell their children to be careful, there is always a case of a kid getting injured. Skateboarding is no exception to this rule - children ride skateboards down hills for enjoyment, but they can lack the strength and skills necessary to maintain a velocity that will not do significant harm to them. Some engineering projects have attempted to mitigate this issue by using simple braking systems; however, there still needs to be a solution that is both simpler and safer. For an electric or motorized skateboard, an automatic skateboard braking system is proposed, which would use several sensors and a microcontroller to automatically force the

skateboard to operate at safe speeds while being operated in conditions that increase the risk for serious injury. (CM)

The proposed skateboard automatic anti-lock braking system, or ABS, would make it much less likely for skateboard and long board riders to sustain injury if riding at higher speed. With the proposed skateboard braking system in mind, it is important to be cognizant of how an ABS system functions for cars, motorcycles, and other similar vehicles. When pressure is applied on the brake pad, a multitude of factors can affect the slowing behavior of the brakes – too much pressure exertion from the vehicle operator or poor environmental conditions, there will be a chance that the wheels lock up. The force exerted on the brakes exceeds the amount of kinetic friction needed to keep the wheels in motion. For quite some time now, the anti-lock braking system has been implemented in order to detect if at least one wheel is about to lock up just before it happens. There are three crucial parts that make up the ABS system: wheel speed sensors, the ABS control apparatus, and the hydraulic modulation apparatus. (BR)

The angular velocity of the wheels of a motor vehicle is an important part of how the anti-lock braking system functions. When the vehicle's wheels are in motion, there are sensors that detect their rotational motion and convert the readings into electrical signals – the signals can be of either voltage or current. Depending on the ABS design, there can be instances where more than one of a vehicle's wheels has a wheel speed sensor attached. The signals generated from these sensors are later used for determining how much slip there is between the wheels and whatever surface the wheels are on – these calculations help form the basis of the ABS sensing whether or not lock up of the wheels will happen. (BR)

The ABS control apparatus is the heart of the entire anti-lock braking system. When electrical signals generated from the rotational motion from the wheels reach this control

mechanism, they are processed in such a way that at least one actuating signal gets passed on to the hydraulic modulation system so that the latter system behaves or responds in a particular manner. More specifically, through preemptive lock detection algorithms, the acceleration of the wheels, the vehicle's translational speed, and other quantities are calculated, with those output signals serving as the control signals to the hydraulic modulation apparatus. A typical ABS control algorithm monitors the rotational velocity of every wheel on the vehicle it is controlling. The control system is particularly looking for significant decelerations in each wheel. When any wheel's rate of deceleration is faster than that of the rest of the vehicle, the control algorithm signals the braking system to release pressure from the respective wheel until its rotational velocity matches the rest of the wheels. Through this process, the algorithm prevents tire skidding, which allows the vehicle operator to maintain control of the vehicle while braking.

(BR)

The hydraulic modulation system consists of several solenoid valves, with one pair of these valves being connected to each brake. These valves are electromechanical, and they can open and close the hydraulic circuits linked to the brake master cylinder. The inlet valve located between the vehicle's brake master cylinder and the brakes regulates how much pressure is being applied, and the outlet valve located between the brakes and the vehicle's return pump regulates the amount of pressure being released. Typically, the inlet valve is open, meaning that there is a direct path between the brake master cylinder and the brakes; thus, the pressure exerted by the brake master cylinder directly propagates to the brakes in each wheel; however, if the slip between the wheels and the surface the wheels are on increases and reaches a certain threshold, the direct connection previously formed shuts off in order to cut off any rise in pressure at the brakes from the brake master cylinder. If there is still pressure build-up at the site of the brakes,

the outlet valve opens in order to allow the return pump within the hydraulic modulation apparatus to draw brake fluid in a regulated fashion. Therefore, the pressure in the relevant brake(s) is significantly reduced to levels safe enough that the brakes do not lock up. With the mechanics of hydraulic brakes from large scale vehicles taken into consideration, it is proposed that a similar type of apparatus be designed using solenoids instead of hydraulics. The use of induced currents generated by changing magnetic fields through the metal coils, which generate impedances, will act as the mechanism that changes the pressures between the different parts of the brakes. (BR)

There are two different types of skateboards where braking is used: electric boards and mechanical boards. With respect to the former, the braking system is implemented into the electronic drive system, with dynamic braking to regenerate battery energy. If the skateboard moves too quickly, then the ABS disables to prevent the generation of excess current from the regenerative braking. It should be noted that braking for electric skateboards can only occur while the skateboard battery has a charge. This type of braking system can be found on branded models such as Boosted and Mellow Drive Boards. The alternative is a system provided by Brakeboard – a mechanical brake is installed through the board, giving a physical pedal that applies the braking mechanism upon receiving a downward force. At the same time, the braking can only be achieved by the skateboard user when he or she is able to press down on the device. (RH)

The proposed skateboard braking system design already has competitors prevalent throughout the market. These competitors have identifiable differences and similarities to the suggested skateboard braking system. For instance, fully electric skateboards include a system to analyze and control the speed of the board; but, the suggested anti-lock braking system will use a

control algorithm to add automated braking functionality. In addition, the proposed skateboard ABS system will use motors connected to each wheel in order to control their braking – a similar approach to braking systems currently on the market. Also, an anti-lock component will prevent skidding, allowing the user to maintain control of the board. The proposed design will include a mechanism to inform the user of the charge on the battery. (RH)

There are multiple patents that are pertinent to the concepts outlined in the proposed skateboard anti-lock braking system. For example, Yik Hang Pang’s 2018 patent for an “electrical transportation tool” consists of a design for a concept motorized skateboard. Another patent that pertains to the ABS system is the 2007 patent for an “antilock and antiskid mechanical brake system for vehicles,” which consists of a design for a mechanical antilock braking on a smaller-wheeled vehicle such as a bicycle (Pang). The method used for the brake system is described as “vice grip brake arms” and is a viable alternative to the hydraulic antilock braking system (Peles). The patents previously discussed are a sliver of the innovation that anti-lock braking systems have provided for vehicles of many types. (LM)

Anti-lock braking systems have been revolutionary in keeping drivers safe as they travel from place to place via car, motorcycle, etc. This invention, combined with the fact that children and teenagers have been injured in skateboarding incidents, therefore has led to the proposal of an automatic skateboard anti-lock braking system. While there are electric skateboards that have braking systems already, this design will be much safer and more straightforward, drastically diminishing the chances of somebody sustaining an injury on a skateboard. (CM, BR)

## 1.4. Marketing Requirements

Table 1 shows the marketing requirements that need to be met for customer satisfaction and safety.

Table 1: Marketing Requirements

Marketing Requirements	
1	The longboard system will prevent the user from traveling at unsafe speeds
2	The longboard system can be used on hills
3	The longboard system will not cause the rider to be ejected from the board
4	The longboard system will indicate to the user when braking is engaged
5	The longboard system will be self-powered and portable
6	The longboard system will have automatic anti-lock braking

## 2. Engineering Analysis

### 2.1. Batteries (BR)

Batteries are critical components of many portable electronic systems and devices, including the automatic longboard braking system – they provide the energy and power needed to drive said systems. There were several factors that were examined in order to decide the most optimal battery to use for the longboard automatic anti-lock braking system: charge capacity, cell chemistry, rated voltage, charge cutoff voltage, discharge cutoff voltage, and cycle/service life. Charge capacity refers to how much charge a battery can supply to a load before becoming depleted. In order to figure out how much charge to supply to a load, which, assuming low enough currents, is

$$Q_{batt} = I_L t \quad , \quad (1)$$



where  $Q_{\text{batt}}$  is the battery capacity,  $I_L$  is the load current, and  $t$  is time. Cell chemistry refers to the materials used for the anode and cathode electrochemical reactions, which can have consequences on many of the other parameters. Rated voltage is the voltage batteries are marketed at – they can be a few hundred millivolts smaller than the charge cutoff voltage, which is the battery voltage when fully charged. Discharge cutoff voltage is the voltage at which a battery becomes “dead”. Cycle/service life is for how many cycles, on average, a battery can be used for until it needs replacing. This parameter is dependent on discharge currents and at what percent capacity a battery was tested at. For the longboard application, rechargeable batteries were of the most interest, as they are much more widely used nowadays and much more energy-efficient and cost-effective than non-rechargeable batteries.

When analyzing different battery technologies, their respective advantages and disadvantages, as well as their typical voltage and charge capacity parameters, were noted. For lead acid batteries, they are very durable, tend to be economically priced, and have high charge capacities. At the same time, however, they have a limited number of charge and discharge cycles before needing to be replaced. Lead acid cells typically have rated, charge cutoff, and discharge cutoff voltages of 2 V, 2.4 V (sometimes, however, they can hover around 2.25 V), and 1.75 V, respectively. In addition, lead is poisonous to humans and can pose health risks. Nickel-cadmium (NiCd) batteries are some of the most durable batteries manufactured, and they are often used when high current discharge rates, extreme operating temperatures, and high service life are critical. The downside of this type of battery, however, is that can cause environmental concerns. NiCd cells are usually rated around 1.2 V, carry a maximum voltage of about 1.55 V, and need to be recharged once they drop below 1 V. Nickel-metal-hydride (NiMH) batteries have higher specific energies than NiCd with the same voltage properties; however, even though the former

uses metals that are significantly less dangerous for the environment, they can still be somewhat toxic. Lithium-based batteries come in different varieties: Lithium-Ion (Li+) and Lithium-Polymer (LiPo). These two types of batteries are more expensive, but they can last longer in terms of cycle count, and they are more lightweight. In addition, these two cell types require less maintenance than other types. Some of the added expense also comes from the fact that lithium-based batteries are manufactured with specially-designed protection circuits – these types of cells are very sensitive to overcharging and over-discharging and can cause severe safety hazards, and their normal charge and discharge currents are typically rated at around 0.2C (20% of the charge capacity). It is important to note that while Li+ and LiPo batteries have similar characteristics, their voltage and charge capacity values are typically different. Additionally, Li+ batteries are typically manufactured with cobalt, manganese, or phosphate. For LiPo cells, and for Li+ cells made with cobalt and manganese, the rated, charge, and discharge cutoff voltages are usually around 3.6 to 3.7 V, 4.2 V (and sometimes higher), and between 2.5 and 3 V, respectively. For Li+ cells made with phosphate, however, those voltage parameters are typically around 3.2 to 3.3 V, 3.6 V, and 2.5 V, respectively.

When it came down to choosing what battery type to use, it was determined that a LiPo cell was optimal for the longboard braking system. The long cycle lives of these cells on average, not having to worry as much about potential the over-discharging or over-charging of cells due to built-in protection circuits that disconnect the cell electrodes in such cases were two of the main factors that contributed to the selection. The long cycle life makes it so that cells do not have to be replaced frequently – a convenience for the user. Also, there is not that much space along the length or width of longboards. Attempting to attach a battery holder to the bottom of a longboard could add enough mass to impact other parts of the longboard braking system. The compactness

and lightness of LiPo batteries, coupled with the fact that many of them, like the PRT-13813, come in thin, rectangular packages and with external wires attached to their respective electrodes, helps keep the total mass of the combined longboard-longboard system to a minimum and the combined system center of mass more stable. Also, it was decided that a supply voltage of 3.3 V was going to be used to power the other components discussed later on; thus, one compact Li+ cell of nominal voltage 3.7 V was a good starting point – See Section 2.2.2 for more details.

## **2.2. Electronics**

### **2.2.1. Charge Management (BR)**

There were various techniques that were investigated when figuring out how to best charge the batteries being used for the longboard braking system while taking overcharging/overvoltage risks into consideration: Constant current (CC) charging, constant voltage (CV) charging, constant voltage/constant current (CVCC) charging, and smart charging. CC charging, which utilizes a small, constant current to charge a battery all the way through, is simple to implement. Charging stops when predetermined voltage value is met. It is important to note, however, while much higher currents charge a battery faster, the battery will age much more rapidly. On the other hand, while much lower currents make better use of a battery's charge capacity capabilities, that battery will take significantly longer to charge. CV charging is done by setting a constant voltage to charge a battery. This advantage of choosing CV charging is that overcharging can be avoided due to the charge current decreasing as the battery charges. CV charging is also generally very time-efficient; however, because the required current for fast charging at earlier parts of the charging process are relatively high, electrical overstress (EOS) on the battery can cause battery lattice frames to break

down. CVCC charging is a hybrid combination of CC and CV charging. When utilizing this technique, a battery first charges via CC charging until reaching a predetermined battery voltage value. Once that threshold is reached, the battery switches to CV charging. This charging method can be thought of as a compromise between charge time – typically influenced by the CC stage, and charge capacity capabilities – typically influenced by the CV stage. CVCC charging is very beneficial in the sense that it is more efficient than either CV or CC charging individually; however, determining the most suitable voltage to switch between charge stages remains difficult when balancing charge time efficiency and charge capacity capability. Additionally, if Li-based batteries are being charged, then CC charging generally needs to be for a longer period. It should be noted that if more than cells are connected series, then unless they are being charged very slowly, a separate charge balancing circuit need be designed to ensure as ideal voltage matching as possible.

There are many different solutions being employed today with respect to managing a battery during its charging process. Charge management integrated circuit (IC) technology is quite common. Further, charge control ICs can be separated into three different types: Linear, switching, and pulse. Linear and switching chargers have similar merits and drawbacks as voltage regulators – these two types of charger ICs typically integrate internal regulators when setting voltage thresholds for when to exit precondition mode (charging a battery at only a small fraction of the desired charge current when the battery voltage is around the discharge cutoff value) and/or when nearing the end of charging. Linear charge controllers like the MCP73213 are simpler in design, smaller and less susceptible to electromagnetic interference (EMI), but can have poor power efficiency. From the MCP73213 datasheet, the maximum power dissipation  $P_{d,max}$  can be approximated with

$$P_{d,max} \approx I_{chg}(V_{DD} - V_{TH,min}), I_{chg} \gg I_Q, \quad (2)$$

where  $I_{chg,max}$  is the maximum charging current,  $V_{DD}$  is the active supply voltage,  $V_{I,min}$  is the minimum threshold voltage when transitioning between precondition mode CC mode, and  $I_Q$  is the quiescent current – this current is assumed to be much smaller than  $I_{chg,max}$ . Switching charger ICs are more power-efficient, but they are more susceptible to EMI and take up more room since large, passive LC filters are needed to remove any interference. The filter addition also makes switching charger designs more complicated. Pulse chargers are a hybrid between the two previously discussed charger types – they dissipate much less power and do not require any filtering; however, they typically require specially-designed current-limiting AC/DC adapter technology. Regardless of type, most, if not all, of the charge controller ICs that were looked at also have dedicated pins so that battery or battery pack voltages can be easily monitored while charging, as well as either push-pull or open-collector/drain status pins for telling the user whether those batteries or battery packs are, charging, done charging, or not charging due to a fault occurrence. The faults can range from overvoltage, overcurrent, over-temperature, no presence of a battery or battery pack, and internal timer expiration.

For charging the braking system batteries, it was decided that a linear, CVCC charge controller would be used. In order to conserve as much mass and space as possible underneath the longboard, external inductors were not practically feasible. Additionally, the simplicity of linear ICs makes it so that there is relatively simple external circuit design – one can set the desired CC current just by changing a single external resistance for many of them. CVCC is also a very safe and relatively fast technique of charging LiPo cells. Because of constraints related to the voltage regulator – see Section 2.2.2, two cells and a dual-cell charge controller were decided to be used. Also, due to charging ICs have ranges of allowable CC charge currents, and due to power

dissipation stipulations in linear chargers, the current and battery pack capacity would have to be carefully selected in order to assure no damage to the regulator, the battery pack, or the charge controller. For example, if the longboard control system were to require 100 mA to power the electronics, then, assuming discharging at 0.2C, the charge capacity would be 500 mA·h using Equation 1. Then, assuming charging at 0.5C using an MCP73213 controller, the CC charge current would be 250 mA using Equation 1. At the same time, assuming the battery pack voltage is low enough, the IC would dissipate about 750 mW of power – Equation 2 was used here. While power is a key parameter to monitor, the merits of the linear, CVCC charge controller vastly outweigh the negative aspects.

### 2.2.2. Voltage Regulation (BR)

Voltage regulators are responsible for maintaining a constant DC voltage regardless of current. This is crucial in the context of using batteries, or for that matter any power supply, when the components that need to be energized need a very specific voltage or can only tolerate a specific voltage range. As previously alluded to in the charge control discussion, there are two different types of voltage regulators: Linear and switching. The pros and cons for these regulators are pretty much the same as those of the charger IC technologies. What was not included, however, was that linear regulators are typically only able to step down voltages, while switching regulators can be designed to both step up and step down voltages. Equation 2 can be renamed to reflect the general case for a voltage regulator:

$$|P_{d,max}| \approx I_L(V_I - V_{reg}), I_L \gg I_Q, \quad (3)$$

where  $V_I$  and  $V_{reg}$  are general input and regulated voltages, respectively. Additionally, there are special types of linear voltage regulators called low dropout regulators (LDOs), which can regulate input voltages even if they are very close to the regulated output voltage. It should be noted that there are current limits for both types of regulators.

For the longboard braking system, as previously mentioned, a 3.3 V supply voltage was decided to be used to power most of the other electronic devices. Because the discharge cutoff voltage for a Li+ cell is around 3.0 V, a single 3.7 V cell would not suffice; thus, putting two LiPo cells in series to create a two-cell battery pack was determined to be a good way to mitigate that issue. The total charge cutoff voltage across two LiPo batteries is around 8.4 V, and the total discharge cutoff voltage across both cells is around 6 V, so the regulator will be able to provide a stable 3.3 V to the other electronics. When considering heat dissipation, if a load current of 100 mA was assumed to be driven through a linear regulator when using the battery pack described before, then according to Equation 3, then the maximum power dissipation, which occurs when both cells are completely charged, would be 510 mW. These calculations led to the decision to include a heat sink on the chosen linear regulator in order to better dissipate the heat from the device. The heat sink would be chosen based off the device package and the maximum device junction thermal resistance  $\theta_{JA}$  listed on the regulator datasheet.

## **2.3. Sensors**

### **2.3.1. Wheel Speed Measurement (BR)**

Accurately measuring the angular speed of longboard wheels is essential for determining if the longboard is traveling too quickly with respect to linear velocity, as well as for determining

whether the wheels are slipping or skidding or not. Tachometers are commonly used to measure angular speed; however, for the longboard, it would take up too much space. There are other types of devices that showed promise in being able to precisely measure longboard wheel speed: Hall effect sensors, magnetoresistive sensors, inductive sensors, and optical sensors. Hall effect sensors operate on the basis of the Hall effect – an external magnetic field perpendicular to a (semi)conducting surface exerts a magnetic force on positive and negative charge carriers, causing them to concentrate on separate sides of the material, creating a potential difference. This can be accomplished either through currents or through permanent magnets. These types of sensors are designed to be either unipolar – only one face of the sensor can sense a change in magnetic field – or omnipolar – both faces of the sensor can sense a change in magnetic field. Magnetoresistive sensors utilize magnetoresistive materials – when an external magnetic field is applied, the electric resistance of those materials can be altered – and can be designed on a semiconducting material. An inductive sensor works on the concept of electromagnetic induction – an EMF is induced when there is a change in magnetic flux. The pitfalls of this sensor, however, are that they tend to be larger in both size and mass due to the inductive coils and housings used. Optical sensors operate based on the photoelectric effect, which is when photoelectrons, therefore currents, are produced from light photons. This type of sensor can be placed at a larger distance away from a target than other sensors like the Hall effect sensor; however, the longer-range sensors tend to be significantly larger in housing size and price.

The output signals of these different sensors on their own are generally very small and impractical from a longboard wheel speed measurement perspective. Fortunately, many of the types of sensors discussed above have signal conditioning/processing systems integrated with the sensing material all on one semiconducting chip that allow for several output types. There are



sensors that allow for interfacing with microcontrollers, analog-to-digital signal outputs, and logic pulses. For the longboard wheel case, it was determined that in order to accurately measure wheel speed, a logic output could be used with a sensing system that could continuously measure a moving target passing a fixed point once per wheel revolution. If a target were to move into the vicinity of a sensor, like the AH1806, and a parameter like the magnetic field intensity was high enough, then the output of that sensor would change state. Conversely, if the target were to move out of the vicinity of that sensor, then the sensor output would revert to the original logic state. Putting those two cases together would result in a pulse once every wheel revolution, yielding a pulse frequency  $f_{pulse}$  proportional to the longboard wheel velocity  $\omega_{wheel}$ :

$$f_{pulse} = \frac{\omega_{wheel}}{2\pi} \quad (4)$$

In the end, because of the lightness, simplicity, and compactness of the device, a Hall effect sensor was the ideal choice for measuring wheel speed. It was also determined that to reduce the amount of potential EMI, a unipolar sensor was chosen over an omnipolar sensor. In order to be able to get sensor readings, it was decided that at least one neodymium iron boron (NdFeB) magnet would be mounted onto each of the rear wheels – cylindrical NdFeB magnets were selected since they are very common with respect to smaller sizes and had much simpler equations associated with them compared to other geometries. The magnets were chosen based on their size and their sensing distance relative to the magnetic field trip points of the Hall effect sensor (a small magnetic field trip point to turn the sensor on was more ideal). The sensing distance was calculated from graphing

$$B(z) = \frac{B_r}{2} \left[ \frac{z + L}{\sqrt{R^2 + (z + L)^2}} - \frac{z}{\sqrt{R^2 + z^2}} \right] \quad (5)$$

$B_r$  is the remanent/residual magnetic flux density,  $R$  is the radius of the magnet,  $L$  is the thickness of the magnet,  $z$  is the distance from the center of the magnet in the axial direction, which was taken to be the  $z$ -axis, and  $B(z)$  is the magnetic flux density at any point on the  $z$ -axis, since that is the only component of the magnetic flux density that exists. Because magnet datasheets typically only give surface fields, i.e.  $B(0)$ ,  $B_r$  had to first be figured out using

$$B_r = 2B(0) \left( \frac{\sqrt{R^2 + L^2}}{L} \right). \quad (6)$$

It should be noted that Equations 5 and 6 neglected fringing and potential stray fields. Figure 1 shows plots of  $B(z)$  (in mT) as a function of  $z$  (in mm) for some of the magnets that were looked at.

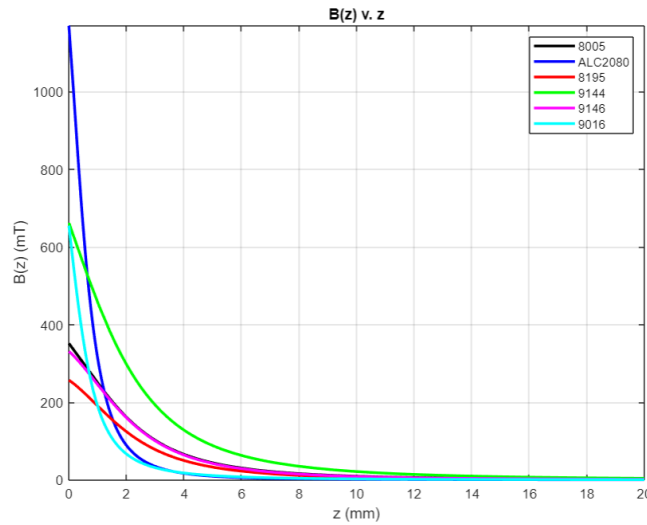


Figure 1: Magnetic Flux Densities v. Axial Distance

As stated before, the sensing distance depends on the Hall effect sensor magnetic field trip point and the magnet's geometry and remanent field. For instance, the AH1806 omnipolar Hall effect sensor switches logic states when it senses at least  $\pm 4.5$  mT and switches back to the original state when the sensed magnetic field drops below  $\pm 4$  mT. From Figure 1, for an 8005 magnet

coupled with an AH1806, the distance at which the magnetic flux density was about 4 mT was when the magnet was about 1.3 cm away from the sensor. For the longboard application, because it was decided that there would be some mechanical hardware underneath the board, the sensing distance did not have to be very large; therefore, a magnet and Hall effect sensor combination that yield a sensing distance of around 2 cm was sufficient – it was also determined that that could be done, despite restrictions with respect to longboard wheel sizes and the space underneath the longboard. One issue that had to be considered and was not discussed previously, however, was response/delay/refresh time. Some sensors, like the AH1806, have an “on” time on the order of microseconds, but a period on the order of milliseconds (typically around 75 ms for the AH1806). Other devices, like the AH3362Q, have a response time delay – the time it takes the sensor to switch logic states when either of the two magnetic field thresholds are passed – on the order of microseconds (typically 3.75  $\mu$ s for the AH3362Q). A longer response time may result in the chosen Hall effect sensor not consistently sampling the speed of the longboard wheels if the wheels are spinning quickly enough. From preliminary testing, it was empirically determined that a very short response time like that of the AH3362Q is needed for measuring faster wheel speeds. It was also decided that there would be to be two Hall effect sensors – one per rear wheel – to figure out if slipping or skidding occurs.

To test the Hall effect sensor proof of concept, three 9144 NdFeB disc magnets were lined up next to each other inside a metallic drum, and the drum was connected to a drill. The drill was set to different speeds, the corresponding Hall effect sensor pulses were measured with an oscilloscope. The angular speed was then measured with a tachometer, and the angular frequencies were compared. The Hall effect sensor pulse frequency was measured to be about

21.74 Hz, which is about 1304 rpm. From the tachometer, the measured angular speed was 1281 rpm – an error of about 1.80%. A waveform capture from the oscilloscope is shown in Figure 2.

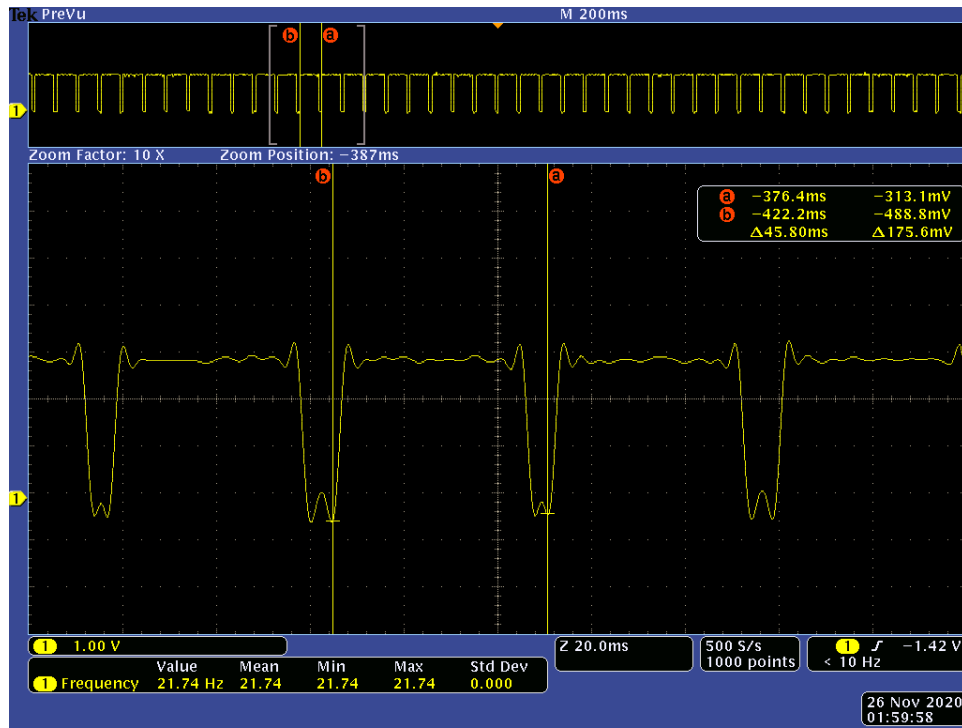


Figure 2: Hall Effect Sensor Waveform

Based on the measured frequencies and waveforms, it is possible to use a Hall effect sensor to measure wheel speed; however, the noisiness of the signal needs to be considered.

### 2.3.2. Angle of Elevation Measurement (CM)

The angle of elevation measurement can be obtained through the usage of the gyroscope sensor in the IMU. The measurement would then be sent over a bus protocol such as I2C. However, more needs to be done with the sensor data to convert it to useful information. For example, in an LSM9DS1 IMU, the datasheet specifies that a measurement range should be chosen. The units used for the measurement range are a rate of angular change, degrees per second

(dps). The measurement range can be set to  $\pm 200$ ,  $\pm 500$ , or  $\pm 2000$  dps. The output value of the gyroscope is a 16-bit integer expressed in two's complement. The higher the chosen range is, the lower the resolution is. In the case of this project, the lower 200 dps range should be chosen since the maximum incline is around four degrees, and a rate about 200 dps to reach such an angle is unrealistic. When a reading from the gyroscope is taken, the next step is to convert that value into useful information for the rest of the system. Such a conversion is realized through integrating the values with respect to time. A value keeping track of the current angle, combined with a time multiplier scaling the rate of angle change to total angle change, would be required to calculate the angle of descent. However, an issue worth noting is the accumulation of error. Every iteration has a slight error and by adding error on every iteration, the calculated angle of descent will drift from the true physical angle. An accelerometer could also be used to calculate the angle of descent, considering that gravity has an acceleration of 1 g; but, the downside to this method of angle calculation is the linear acceleration that could be caused by the rider kicking to propel the skateboard forward. In this project, a complementary filter will be used to combine the best of both sensors. The angle value obtained by the gyroscope would be passed through a high-pass filter and the angle obtained by the accelerometer would be passed through a low-pass filter. The gyroscope values are high pass because they provide insight into what angle the board is immediately rotating toward. On the other hand, the accelerometer is values are low pass because the accelerometer provides acceleration information, which is highly varying except for the constant gravitational acceleration pulling the longboard down. Predictive calculations of what velocity the board is approaching in a short time interval can be made to trigger braking earlier than typical braking events would occur. This would limit the energy the system gains early on and prevent the need to dissipate power at a rate higher than the rate at which kinetic energy is being added to the system.

The need for early braking will be characterized by what the velocity could be if the system accelerates at the calculated rate after 100 ms. Mathematically, this means the future velocity is the current acceleration multiplied by 100 ms then added to the current velocity. In other words, the software will integrate the acceleration with respect to 100 ms to obtain the growth in velocity, and then add the current velocity to obtain the board's velocity 100 ms in the future.

#### **2.4. Communications (CM)**

In an embedded sensor system such as this, communication between the embedded processor and sensor is critical to the operation of the system. The sensor data need to be communicated to the host processor. Such communication is realized through the usage of standard communication protocols – Inter-integrated Circuits (I<sup>2</sup>C), Serial Peripheral Interface (SPI), and Universal Asynchronous Receiver/Transmitter (UART), to name a few. Simple analysis reveals that SPI is the simplest and most reserved choice for this project. A simple comparative analysis of the protocols is necessary to reach a conclusion on which one suits the project best.

UART is a simple protocol choice for devices that need to communicate on a one-to-one basis. Standard UART consists of two communication lines: one for receiving and one for transmitting. This keeps communication simple, which is an advantage when working on projects in time constraints. Additionally, UART can offer hardware flow control, which utilizes two additional pins to allow the devices to “handshake” before initiating communication. With such simplicity comes disadvantages as well – UART has a maximum clock speed of one megabaud, though most devices support a baud rate of 115200 or lower. If the baud rate of a device exceeds the supported baud rate of another, then the behavior of the received transmission will be unwieldy,

and the message will vary significantly from the intended message. The greatest disadvantage of UART in the case of this project is that it is not a bus. Theoretically, with enough flow control, UART could be a bus, but implementing such flow control while having a clock speed as slow as typical UART defeats the purpose of the simplicity of UART. Other viable options should be bus protocols, considering that most sensors support busses over UART, busses can transmit data to and from multiple devices, and busses have the advantage of higher transmission speeds.

An example of a bus protocol is I<sup>2</sup>C. I<sup>2</sup>C is a simple bus protocol because it only requires two transmission lines to operate, regardless of the number of devices transmitting on the bus. I<sup>2</sup>C can support clock speeds of up to 3.4 MHz, but many sensors, including the IMU sensor of choice, support up to 400 kHz. I<sup>2</sup>C can support up to 128 devices, which is significantly more than enough devices being used for this project. The I<sup>2</sup>C protocol also specifies starting and stopping conditions, addressing schemes, and read or write bits. This means that, if I<sup>2</sup>C is implemented in the microcontroller, there is only a need to write interfacing code rather than try bit-banging, implementing flow control, etc.

The last protocol that was analyzed was SPI. SPI offers similar advantages to I<sup>2</sup>C in terms of allowing multiple devices to communicate on the same bus; however, SPI offers a higher clock speed, simultaneous bidirectional communication. A disadvantage to SPI is the need to implement slave select lines, since there are no built-in addressing schemes. Such implementation requires the usage of GPIO pins thus requiring more developer time. An important consideration is also whether SPI is specifically needed in this design. According to engineering requirements, the system must make braking decisions every 100 ms, which is enough time for floating point calculations while also being faster than the average human reaction time. Since the IMU readings are a dependency in every 100 ms iteration, IMU readings and bus communications must be taken

only once every 100 ms. Considering that there are only two sensors reading values to the bus and that the physics calculations only need to be made at most once every 100 milliseconds, neither I<sup>2</sup>C nor SPI would become a specific bottleneck.

With these considerations in mind, I<sup>2</sup>C is the bus protocol of choice since it is less work for development for virtually the same benefits as SPI in this project.

#### **2.4. Electromechanics (RH)**

The system will use two motors connected to the rear wheels of the long board. The motors will be used to transform the mechanical energy generated by the movement of the longboard's linear velocity into electrical energy by using the motors as generators. This can be achieved by connecting the shaft of the motor to the wheels through a set of pulleys and belts or with a hub motor. To be able to create enough room for the components, the pulley and belt design will be used. As the wheels rotate, they cause the pulleys on the wheel to drive the belts and rotate the set of pulleys connected to the shaft of the motor. When this system is used, a gear ratio is employed to decrease the torque applied to the motors. A turns ratio of 36 to 16 will be used, with the large gear being attached to the wheel and the smaller gear being attached to the shaft of the motor.

To calculate the maximum torque applied to the motor, a frictionless environment was assumed, and criteria for maximum load was established: a combined weight of 200 pounds traveling at a constant velocity of 12 miles per hour (mph) down a hill with a decline of 4° on a longboard with 90 mm diameter wheels. Initially, 12 mph was converted to meters per second:

$$m/s = MPH/2.2369362920544 \tag{7}$$

Next the weight, in pounds, was converted from pounds-force to Newtons:



$$Force[N] = weight[lbs] * 4.444822 \quad (8)$$

The power generated could be calculated as

$$Power[W] = Force[N] * velocity[m/s] * \sin(angle) \quad (9)$$

The 90 mm wheels have a circumference of 0.2827 m and allows for finding the angular speed of the wheels in revolutions per second (rps).

$$RPs_{wheel} = velocity[m/s] / circumference \quad (10)$$

The angular speed at the wheels would be sent through the pulleys and belts to the gear at the motor, giving the angular speed at the motor. The pulleys at the wheel and motor give a turns ratio, TR, of 36 to 16:

$$RPs_{motor} = RPs_{wheel} * 36/16 \quad (11)$$

To calculate the torque at the motor, the angular speed at the motor needs to be converted to an angular speed  $\omega$  in radians per second:

$$\omega = 2 * \pi * RPs_{motor} \quad (12)$$

The torque  $\tau$  is found by,

$$\tau = Power[W] / \omega \quad (12)$$

where  $W$  is the generated wattage. When divided equally between the motors, a torque value of 0.6206 N·m is seen at the shaft of the motors, and a power of 166.5 W per wheel will be generated by the motors. This leads to the conclusion that to maintain the speed of 12 mph, the system needs to disperse 166.5 W per wheel in a frictionless environment, and as the rider and device with a combined total weight of 200 pounds descends a hill with a 4° incline, 166.5 W of

electrical power will be generated. This energy associated with this power generation is the potential energy being converted to kinetic energy. This energy needs to be dissipated from the system in to maintain 12 mph, which is going to be accomplished by sending the electrical energy from the generator into power resistors to generate heat. To control the system, a signal will be sent from the embedded system to a power transistor. Depending on the established conditions, the signal will be able to disperse a limited quantity of energy, allowing for control of the wheel speed.

In a demonstration, two motors were coupled with a flexible couple. This allowed one motor to act as the driving motor powered by a power supply unit and the second motor to act as a generator. In the demonstration, it was shown that 2.205 V at 13 mA was generated in the second motor when allowed to generate without a feedback emf or additional load. When connected into the circuit, the voltage dropped to 1.900 V, and when connected to 0.5  $\Omega$  of resistance, the voltage generated dropped to 1.241 V. The added torque from the circuit made a noticeable difference as the driver motor slowed down.

## **2.5. Embedded Systems (LM)**

Due to experience with PIC24F controllers and the fact that the boards are relatively accessible, the PIC24F lineup was the first choice in terms of what controller to use; however, the board still needed to satisfy the physical requirements of the project in order for it to be a practical choice.

First and foremost, the board must have a clock speed sufficient to read all sensor outputs while still computing algorithms without invoking a race condition for velocity or acceleration

readings. To find out the target frequency to achieve this, the frequency for the sensors must be considered. For Hall effect sensors, the maximum speed accounted for is 12 mph, which translates to 5.36 m/s. With a 100 mm diameter wheel, this roughly estimates to 17 revolutions per second, or 17 Hz. Moreover, Hall effect sensors are commonly found to have an update frequency that is directly proportional to the speed it is sensing, scaled by  $2\pi$ . This means that at most, the Hall effect sensor will be updating at a rate of around 100 Hz. Knowing that the controller will be running at frequencies in the MHz range, there is no concern in accommodating for this sensor. To receive data regarding the angle of the board, this controller will be taking inputs from an Inertial Measuring Unit, or IMU. The IMU chosen, the BMI088, operates at two speeds when communicating in I<sup>2</sup>C – 100 kHz Standard mode and 400 kHz Fast mode. Considering the controller will only deal with two Hall effect sensors and one IMU sensor in interrupt protocol, even the slowest microcontroller will be able to handle this process with ease.

Another important factor to consider when choosing a microcontroller is I/O support. As previously mentioned, the communication protocol of choice for this project is I<sup>2</sup>C. According to the datasheet for the PIC24F series microcontrollers, they do support I<sup>2</sup>C communication.

### 3. Engineering Requirements Specification (RH, LM, CM, BR)

Table 2 shows the longboard braking system engineering requirements that need to be met, which were derived from the marketing requirements, and their justifications as to why they need to be met.

Table 2: Engineering Requirements with Marketing Requirements and Justification

Marketing Requirements	Engineering Requirements	Justification
5	The system will have a rechargeable power source and will fully charge within a 4-hr. time frame.	Based on battery research the longest charge time of any of the battery choices.
5	The system will have a minimum operational time of 1 hour.	Based on average commuter time, a one-hour charge will provide several days of use.
1	The system will disengage if either of the rear wheels stop moving.	Safety factor to prevent the injury to the rider.
1	The system will engage and disengage within 100 ms.	The time to engage and disengage needs to be faster than the human reaction rate while also being enough time to calculate acceleration and velocity.
1, 3	The system will measure and process the speed of the two rear longboard wheels every 40 ms.	Measuring wheel speed of multiple wheels will help determine slip.
2	The braking system will be able to operate at an angle within the range of 0 to 4 degrees.	A 4-degree angle of descent corresponds to a 7% grade - a common angle at which interstate highway signs warn drivers of potentially high acceleration.
1, 2, 6	The system will dissipate up to 331 W	The system will need to dissipate the energy 200 lbs. total weight at 12 mph descending 4 degrees
1, 2, 3	To prevent ejection of the rider, the g-force applied to the rider during braking will not exceed 1.5g.	It is not the intention of the design to injure the user.

		g-force calculations determined the user would be ejected from longboard when a braking force $> 14.4 \text{ m/s}^2$ is applied.
1, 6	Braking to the individual rear wheels will be sufficient to control the speed and slip.	A dual motor system will allow for better control.
1, 4, 6	The system will initialize braking if the calculated acceleration allows the board to travel faster than 12 mph within 100 ms.	The board needs to preemptively limit its acceleration to minimize power consumption.
<ol style="list-style-type: none"> <li>1) The longboard system will prevent the user from traveling at unsafe speeds</li> <li>2) The longboard system can be used on hills</li> <li>3) The longboard system will not cause the rider to be ejected from the board</li> <li>4) The longboard system will indicate to the user when braking is engaged</li> <li>5) The longboard system will be self-powered and portable</li> <li>6) The longboard system will have automatic anti-lock braking</li> </ol>		

## 4. Engineering Standards Specification

### 4.1. Safety (LM)

The biggest safety concern for the project was that braking too aggressively may cause the user of the longboard to get “thrown off” the board due to inertia. To check if this is plausible, the following scenario was derived:

A free body consisting of two rigid bodies (one representing the rider and one the skateboard) is travelling at the specified maximum velocity of 12 mph while traveling down an incline of  $4^\circ$ . It should be noted that  $m_1 \ll m_2$ ; therefore,  $m_1 + m_2$  can be generalized as  $m$ .

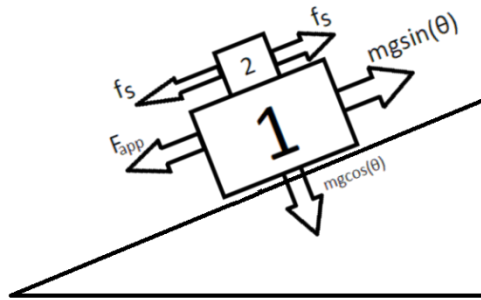


Figure 3: Free Body Diagram of a System Consisting of Two Rigid Bodies

Figure 3 represents the free body diagram for a classical physics problem when encountering two bodies in tandem motion when one gets a local force applied to it: tip or slip? The rationale of setting up this question is the idea that the only way the rider could fall off the skateboard was if they were subject to a force that either caused them to lose balance (tip) or cause their static friction with the board to break (slip). Immediately, tipping can be ruled out because the applied force is applied to an axis that the tipping point of Body 2 is touching. Since the distance between the force  $F_{app}$  and the point is zero, the torque will always be zero no matter how large the force is. The only way the user can tip is if they incorrectly distribute their weight, which then shifts the normal force and gives the board a slight rotational velocity on the user as well; but, it is assumed the user maintains a correctly shifted weight in order to keep both bodies as “rigid”.

With tipping out of the scenario, the slip derivation is calculated. Assuming rolling friction is negligible due to a low moment of inertia on the wheels, the first step is to solve for the total force in the  $x$ - direction for Body 1 (the longboard). This equation ends up being

$$m_1 a_1 = mg \sin(\theta) - f_s - F_{app} \quad (14)$$

where static friction can be converted to

$$f_s = F_{n1,2} = m_2 a_2 \quad (15)$$

By definition, maximum static friction occurs when the directional force is equal to the normal force of the object, meaning

$$m_2 a_2 = m_1 a_1 \quad (16)$$

When substituting Equations 14 and 15 into Equation 16,

$$f_s = mg \sin(\theta) - f_s - F_{app} \quad (17)$$

Readjusting Equation 17 and solving for  $F_{app}$ ,

$$F_{app} = mg \sin(\theta) - 2f_s \quad (18)$$

According to Safety Direct America, a safety grip tape manufacturer, there is a static friction coefficient  $\mu_s$  of 0.77 for non-abrasive standard grip tape. Plugging  $\mu_s$  into Equation 18 and cancelling out the mass gives

$$a_{app} = g \sin(\theta) - 2 * \mu_s g \sin(\theta) \quad (19)$$

$$a_{app} = 9.81 * \sin(4) - 2 * 0.77 * 9.81 * \sin(4) = 14.4m/s^2$$

To break static friction, there would almost need to be 1.5 g's applied to the user. The maximum velocity the board is allowed based on the current model is 12 mph which translates to 5.36 m/s. To achieve this amount of force on the user, the board must brake from maximum speed to a complete stop in less than one third of a second. This is deemed unlikely to happen, so the risk of a user falling off the board due to the system's braking is highly unlikely.

#### **4.2. Data Formats (CM)**

The data used in the project are mostly 16-bit words expressed in two's complement, since that is the format of the data coming from the IMU sensor of choice. The tachometer for this project is interrupt-based, so the data representing its status are single bits for each tachometer.

#### **4.3. Programming Languages (LM)**

The programming language that will be used for this project is C, which was chosen for two reasons. The first being that it is the standard language to be used with PIC24F series microcontrollers. The PIC24F microcontroller has a standard IDE that is used for all Microchip products called MPLAB X. The IDE is ideal to use when programming the microcontroller because it was created to work with the built-in XC8 compiler to program PIC24F controllers using C code. The other main reason C was the language of choice for this project was that it has the least overhead compared to all other compilable, object-oriented, languages. Although C++ is a more common and somewhat regarded to be a "simpler" language compared to its predecessor, C provides the fastest operational solution for an embedded program. Every feature that C++ has over C is due to the extra libraries, which add more behind-the-scenes computations to assist in



programming higher level programs. For a simple embedded program created from scratch, C provides a faster final product that is devoid of any libraries or unnecessary overhead that would only slow the computation down.

## 5. Accepted Technical Design

### 5.1. Hardware Design (RH, LM, CM, RH)

#### 5.1.1. Level 0

Figure 4 and Table 3 correspond to the highest level of the longboard braking system. Figure 4 illustrates the Level 0 hardware block diagram, which details the inputs and outputs to both the charge controller and the control system used for longboard braking. Table 3 provides a list of the designer(s), inputs, outputs, and functionalities for each block. Yellow inputs represent physical signals/data, and red inputs represent external hardware that go into specific subsystems. (BR)

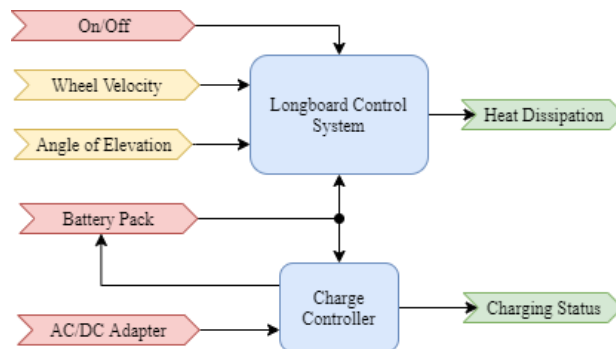


Figure 4: Level 0 Hardware Block Diagram

Table 3: Level 0 Hardware Functional Requirement Tables

<b>Module</b>	Longboard Control System
<b>Designer(s)</b>	Raymond Hoyle, Logan Mashchak, Corey Miller, Ben Roter
<b>Inputs</b>	<ul style="list-style-type: none"> <li>• Wheel velocity</li> <li>• On/off</li> <li>• AC/DC adapter – 9 VDC/800 mA output</li> <li>• Li+ battery pack – 7.4 VDC (nominal)</li> <li>• Angle of elevation</li> </ul>
<b>Outputs</b>	<ul style="list-style-type: none"> <li>• Heat dissipation</li> </ul>
<b>Description</b>	<ul style="list-style-type: none"> <li>• Automatically prevents longboard from exceeding predetermined speed limit and will keep the longboard at that speed until it drops below the limit (without slipping)</li> <li>• Removed energy will be dissipated as heat</li> </ul>

<b>Module</b>	Charge Controller
<b>Designer(s)</b>	Ben Roter
<b>Inputs</b>	<ul style="list-style-type: none"> <li>• 9 VDC AC/DC wall adapter</li> <li>• 2-cell Li-based battery pack</li> </ul>
<b>Outputs</b>	<ul style="list-style-type: none"> <li>• Battery pack charging status</li> <li>• Battery pack charge voltage and current</li> </ul>
<b>Description</b>	<ul style="list-style-type: none"> <li>• Replenishes battery pack voltage and charge without overcharging</li> </ul>

### 5.1.2. Level 1

Figure 4 and Table 4 correspond to the Level 1 Hardware block diagram. Figure 4 illustrates the longboard control system block from Figure 3 being broken down into four different subsystems: voltage regulation, measurement, embedded controller, and brake actuation. Table 4 lists the same type of information as Table 2. (BR)

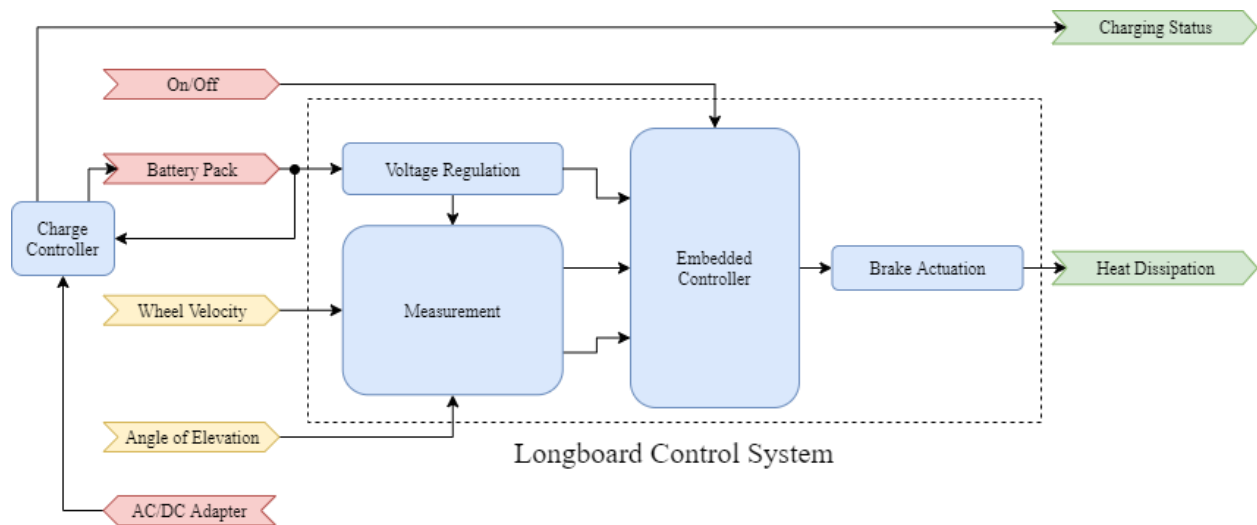


Figure 5: Level 1 Hardware Block Diagram

Table 4: Level 1 Hardware Function Requirement Tables

<b>Module</b>	Voltage Regulation
<b>Designer(s)</b>	Ben Roter
<b>Inputs</b>	<ul style="list-style-type: none"> <li>• 2-cell LiPo battery pack</li> <li>• 9 VDC AC/DC wall adapter</li> </ul>
<b>Outputs</b>	<ul style="list-style-type: none"> <li>• 3.3 VDC</li> </ul>
<b>Description</b>	<ul style="list-style-type: none"> <li>• Supplies stable 3.3 VDC to other electronic devices as battery pack voltage decreases</li> </ul>

<b>Module</b>	Measurement
<b>Designer(s)</b>	Corey Miller, Ben Roter
<b>Inputs</b>	<ul style="list-style-type: none"> <li>• 3.3 VDC</li> <li>• Wheel velocity</li> <li>• Angle of elevation</li> </ul>
<b>Outputs</b>	<ul style="list-style-type: none"> <li>• Pulse of frequency proportional to angular speed of either wheel</li> <li>• Voltage representative of angle of elevation</li> </ul>
<b>Description</b>	<ul style="list-style-type: none"> <li>• Measures angle of elevation and velocity of both rear longboard wheels</li> </ul>

<b>Module</b>	Embedded Controller
<b>Designer(s)</b>	Logan Mashchak, Corey Miller
<b>Inputs</b>	<ul style="list-style-type: none"> <li>• 3.3 VDC</li> <li>• Pulse of frequency proportional to angular speed of either wheel</li> <li>• Voltage representative of angle of elevation</li> </ul>
<b>Outputs</b>	<ul style="list-style-type: none"> <li>• Brake actuation control signal</li> </ul>
<b>Description</b>	<ul style="list-style-type: none"> <li>• Executes predetermined algorithms for slip, linear velocity control</li> </ul>

<b>Module</b>	Brake Actuation
<b>Designer(s)</b>	Raymond Hoyle
<b>Inputs</b>	<ul style="list-style-type: none"> <li>• 3.3 VDC</li> <li>• Mechanical energy</li> </ul>
<b>Outputs</b>	<ul style="list-style-type: none"> <li>• Heat dissipation</li> </ul>
<b>Description</b>	<ul style="list-style-type: none"> <li>• A force will be applied to the wheels increasing friction and controlling to rear wheel velocity</li> </ul>

### 5.1.3. Level 2 (RH, LM, CM, BR)

Figure 5 and Table 5 correspond to the Level 2 Hardware block diagram. Figure 5 illustrates the measurement and brake actuation blocks from Figure 4 being broken down into lower-level systems. The measurement block contains the sensors being utilized in the longboard braking system, and the brake actuation block contains a high-powered switch, a DC motor for each set of wheels, and a load. (BR)

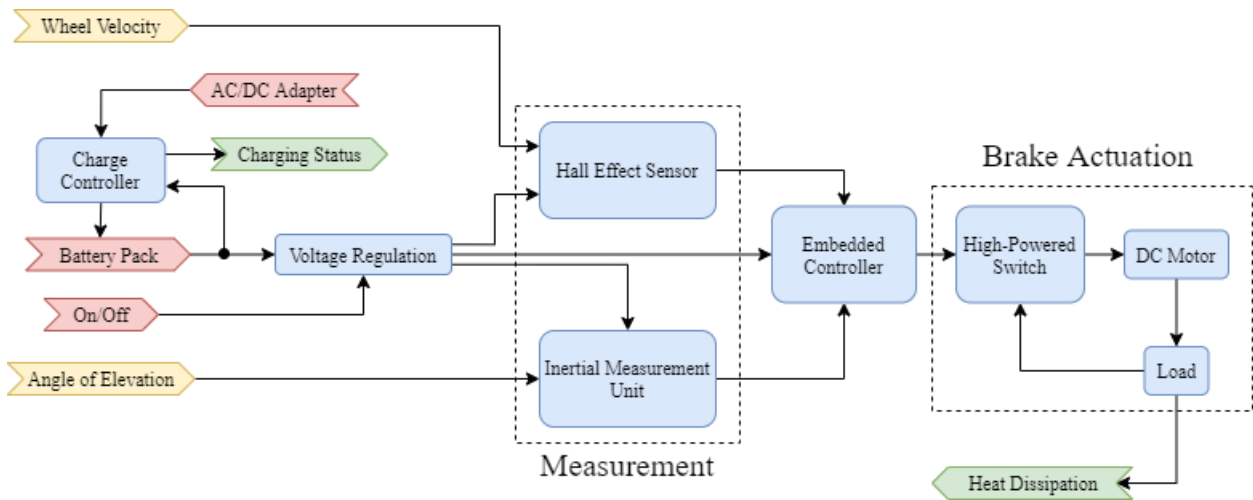


Figure 6: Level 2 Hardware Block Diagram

Table 5: Level 2 Hardware Function Requirement Tables

<b>Module</b>	Voltage Regulation
<b>Designer(s)</b>	Ben Roter
<b>Inputs</b>	<ul style="list-style-type: none"> <li>• 2-cell, LiPo battery pack</li> <li>• 9 VDC AC/DC wall adapter</li> </ul>
<b>Outputs</b>	<ul style="list-style-type: none"> <li>• 3.3 VDC</li> </ul>
<b>Description</b>	<ul style="list-style-type: none"> <li>• Provides stable 3.3 VDC to power other electronics while battery pack voltage decreases</li> </ul>

<b>Module</b>	Charge Controller
<b>Designer(s)</b>	Ben Roter
<b>Inputs</b>	<ul style="list-style-type: none"> <li>• 9 VDC/500 mA AC/DC wall adapter</li> <li>• 2-cell, 500 mA·h LiPo battery pack</li> </ul>
<b>Outputs</b>	<ul style="list-style-type: none"> <li>• Battery pack charging status</li> <li>• Battery pack charge current and voltage</li> </ul>
<b>Description</b>	<ul style="list-style-type: none"> <li>• Replenishes battery pack voltage without overcharging</li> </ul>

<b>Module</b>	Hall Effect Sensor
<b>Designer(s)</b>	Ben Roter
<b>Inputs</b>	<ul style="list-style-type: none"> <li>• 3.3 VDC</li> <li>• Wheel velocity</li> </ul>
<b>Outputs</b>	<ul style="list-style-type: none"> <li>• Electrical pulses of frequency proportional to wheel velocity</li> </ul>
<b>Description</b>	<ul style="list-style-type: none"> <li>• Converts longboard wheel velocities into electrical pulses of frequencies proportional to wheel velocity</li> </ul>

<b>Module</b>	Inertial Measurement Unit (IMU)
<b>Designer(s)</b>	Corey Miller
<b>Inputs</b>	<ul style="list-style-type: none"> <li>• 3.3 VDC</li> <li>• Linear acceleration</li> <li>• Change in rotation</li> </ul>
<b>Outputs</b>	<ul style="list-style-type: none"> <li>• 16-bit two's complement value of linear acceleration</li> <li>• 16-bit two's complement value of pitch</li> </ul>
<b>Description</b>	<ul style="list-style-type: none"> <li>• Reads the values of linear acceleration and changes in rotation</li> <li>• Converts the values into a signed 16-bit integer</li> <li>• Can be scaled to increase measurement range at the cost of resolution</li> </ul>

<b>Module</b>	Embedded Controller
<b>Designer(s)</b>	Logan Mashchak, Corey Miller
<b>Inputs</b>	<ul style="list-style-type: none"> <li>• 3.3 VDC</li> <li>• Pulse of frequency proportional to angular speed of either wheel</li> <li>• Voltage representative of angle of elevation</li> </ul>
<b>Outputs</b>	<ul style="list-style-type: none"> <li>• Brake actuation control signal</li> </ul>
<b>Description</b>	<ul style="list-style-type: none"> <li>• Executes predetermined algorithms for slip, linear velocity control</li> </ul>

<b>Module</b>	High-Powered Switch
<b>Designer(s)</b>	Raymond Hoyle
<b>Inputs</b>	<ul style="list-style-type: none"> <li>• 3.3 VDC</li> </ul>
<b>Outputs</b>	<ul style="list-style-type: none"> <li>• Resistance</li> </ul>
<b>Description</b>	<ul style="list-style-type: none"> <li>• Allows for control of the resistance applied to the output electrical energy from the DC motors</li> </ul>

<b>Module</b>	DC Motor
<b>Designer(s)</b>	Raymond Hoyle
<b>Inputs</b>	<ul style="list-style-type: none"> <li>• Mechanical power</li> </ul>
<b>Outputs</b>	<ul style="list-style-type: none"> <li>• Electrical power</li> </ul>
<b>Description</b>	<ul style="list-style-type: none"> <li>• Transforms mechanical power in the form of angular velocity into electrical power with motor acting as generator</li> </ul>

<b>Module</b>	Load
<b>Designer(s)</b>	Raymond Hoyle
<b>Inputs</b>	<ul style="list-style-type: none"> <li>• Current from DC generator</li> </ul>
<b>Outputs</b>	<ul style="list-style-type: none"> <li>• Heat dissipation</li> </ul>
<b>Description</b>	<ul style="list-style-type: none"> <li>• Power resistor being used to transform electrical energy into heat to be dissipated into the environment.</li> </ul>

### 5.1.4. Hardware Schematics (RH, LM, CM, BR)

To implement the charge controller block, the schematic shown in Figure 7 was designed.

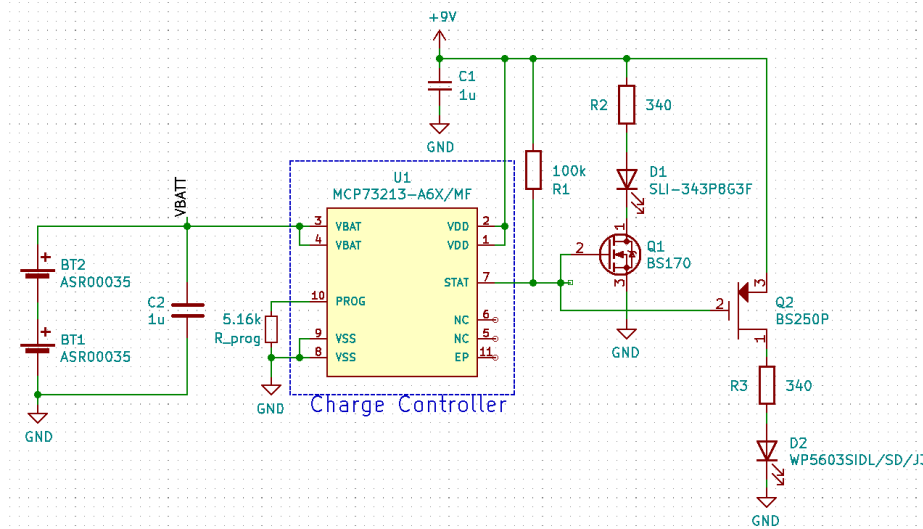


Figure 7: Charge Controller Circuit Schematic

BT1 and BT2 are the two cells in the two-cell battery pack previously discussed, which, to reiterate, has a total nominal voltage of 7.4 V, a total charge cutoff voltage of 8.4 V, and a total discharge cutoff voltage of about 6 V – ASR00035 cells were used. BT2 is connected to the VBAT pins on the controller. Because the two cells will be charged slowly – about 0.48C, a charge balancing circuit need not be implemented necessarily. U1 is an MCP73213 CVCC charge controller – the exact one being used for this design is the MCP73213T-A6BI/MF, which can output a charge current anywhere from about 130 mA to about 1.1 A. It should be noted that the thresholds for setting the CC and CV charging regions are predetermined by the manufacturer. The user can specify the desired CC charge current with the resistor  $R_{prog}$  –  $R_{prog}$  in the schematic – based on the following equation from the charge controller datasheet:

$$R_{prog} = 10^{-\frac{\log \frac{I_{chg}}{1104}}{0.93}} = \left( \frac{1104}{I_{chg}} \right)^{\frac{1}{0.93}} \quad (20)$$

$R_{\text{prog}}$  connects to the PROG pin on the charge controller. For this application, a 500 mA·h battery pack - two was determined to be suitable for the braking system in order to fall within the controller CC charge current range and to make sure the current consumption requirements could be met without damaging the cells. It was decided that 240 mA when charging at 0.48C was a sufficient  $I_{\text{chg}}$  after reviewing the maximum recommended charge rate and providing a little margin due to safety concerns; thus, using Equation 20,  $R_{\text{prog}}$  turned out to be about 5.16 k $\Omega$ . The MCP73213 has an open-drain STAT pin, which outputs the charging status of the battery as a logic signal. Because of the open-drain configuration, pull-up resistor  $R_1$  – R1 in the schematic – is needed to pull the high-impedance state to a logic high. A value of 100 k $\Omega$  was decided in order to minimize the amount of current consumption by the STAT pin’s internal NMOS transistor, which turned out to be about 33  $\mu$ A if the “on” resistance of the transistor  $R_{\text{DS,on}}$  is neglected. That current was calculated using Ohm’s Law as an approximation for the transistor drain current  $I_D$ :

$$I_1 \simeq \frac{V_{\text{DD}}}{R_1}, \quad R_1 \gg R_{\text{DS,on}} \quad (21)$$

$V_{\text{DD}}$  is the supply voltage for the charge controller, which was decided to be 9 V and is discussed in more detail later. When STAT is low, then the battery pack is charging. When STAT is pulled up to high, either the battery pack is done charging or there is a fault that causes the charge controller to stop whatever it is doing. From the device datasheet, if there are instances of overtemperature, overcurrent, overvoltage, lack of a battery pack present, or lack of a resistor to set the CC charge current, or internal timer expiration, then the MCP73213 will stop whatever it is doing, and the STAT pin will be pulled up to logic high – those conditions are factory set. The user will be able to see those signals through the implementation of LEDs. The red WP5603SIDL/SD/J3 LED – D2 in the schematic – means the battery pack is charging, and the



green SLI-343P8G3F LED – D1 in the schematic – means the battery pack is done charging or a fault has occurred.  $R_2$  and  $R_3$  are current limiting resistors for each of the LEDs and are labeled as R2 and R3 in the schematic, respectively. Both resistors have values of  $340 \Omega$ , which were determined by using an LED forward voltage  $V_F$  of 2.2 V at a test current  $I_F$  of 20 mA – those values were from the LED datasheets – and the following approximation of Ohm’s Law:

$$R_{2,3} \simeq \frac{V_{DD} - V_F}{I_F}, R_{2,3} \gg R_{DS,on} \quad (22)$$

It was determined that  $V_{DD}$ , which is fed into both VDD pins on the controller, would be 9 V since that was within the supply voltage range the MCP73213 datasheet specified.  $V_{DD,1}$  is represented on the schematic as +9 V and, in practice, was decided to be implemented using a WDU9-500 9 V/500 mA AC/DC wall adapter. In the schematic, Q2 is a BS250P PMOS transistor that is responsible for turning the red LED on when STAT is low and then off when STAT is high. Q1 is a BS170 NMOS transistor that is responsible for turning the green LED on when STAT is high and off when STAT is low. The maximum total current needed to be supplied by the AC/DC adapter to the rest of the charging circuit was determined to be about 390 mA, which was figured out by summing the two LED currents and the desired CC charge current up; however, to protect against current spikes due to potential parasitic currents, it was decided that an adapter with a current rating of 500 mA would suffice.  $C_1$  and  $C_2$  – C1 and C2 in the schematic – are filter capacitors that were implemented to reduce the effects of potential EMI from high frequency signals. A value of  $1 \mu\text{F}$  was chosen for both capacitors based off recommendations from the charge controller datasheet. The maximum power dissipated by the MCP73213 was calculated to be 720 mW from Equation 2, assuming “precondition” mode. There are no connections involving the NC and EP pins; however, for the it should be noted that there is an exposed pad integrated into the IC package so that when mounted onto a DFN-10 area

of a printed circuit board, which should have a conducting layer underneath the IC, the removal of heat dissipation is more efficient. It should be noted that both charge controller IC VSS pins are connected to ground. (BR)

To implement the longboard control system, which consists of the subsystems discussed previously, the schematic shown in Figure 8 was designed.

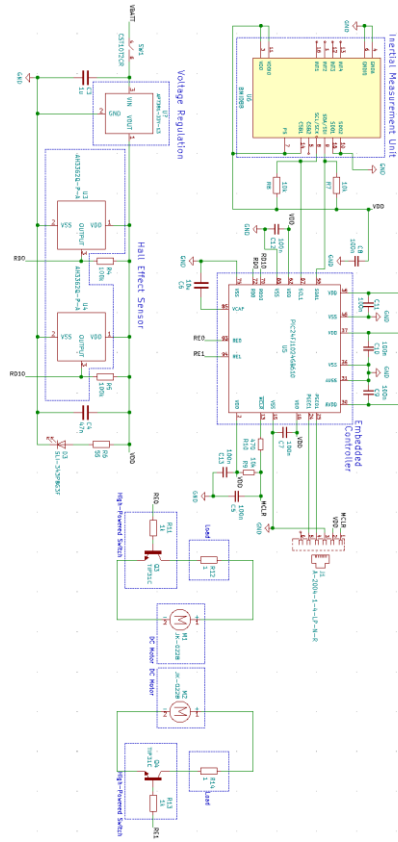


Figure 8: Longboard Control System Schematic

Also, to accommodate an on/off switch so that the user can turn the longboard braking system on and off when necessary, a CST10T2CR toggle switch – SW1 in the schematic – would be implemented. Additionally, a green LED of the same type as the one used in the charge controller circuit – D3 in the schematic – was implemented to tell the user that the longboard braking system is on. The current limiting resistor  $R_6$  – R6 in the schematic – was calculated to

be  $55 \Omega$  under the same  $V_F$  and  $I_F$  conditions ( $I_F$  is the diode forward test current in this case); however, the regulated supply voltage  $V_{reg}$  of 3.3 V mentioned earlier was used, yielding the following Ohm's Law approximation:

$$R_6 \simeq \frac{V_{reg} - V_F}{I_F} . \quad (23)$$

For the voltage regulation subsystem, it was decided that an AP7381 linear regulator, denoted as U2 in the schematic, would work for this application. The VIN pin on the regulator corresponds to the positive terminal of the ASR00035 series battery pack mentioned before, and the VOUT pin corresponds to  $V_{reg}$  of 3.3 V ( $V_{reg}$  is shown as the node label VDD in the schematic). The regulator is responsible for making sure that a stable 3.3 V is available to energize the measurement and embedded controller subsystems regardless of the current. For this regulator, the rated current is 150 mA, and, using datasheets associated with the chosen Hall effect sensor, IMU, and embedded controller, the total current consumption by the measurement and embedded controller blocks was calculated to be about 61.5 mA. In the worst case, the total current consumption  $I_{DD}$  was found by

$$I_{DD} = \sum I_{electronics} = 2I_{HES} + I_{EC,max} + 2I_7 + I_{IMU,acc} + I_{IMU,gyr} + I_F . \quad (24)$$

$I_{HES}$  is the sum of maximum supply and calculated output currents for each of the two Hall effect sensors,  $I_{EC,max}$  is the maximum recommended embedded controller current (not to be confused with the absolute maximum rated current),  $I_7$  is the current through the I<sup>2</sup>C pull-up resistor  $R_7$  – R7 in the schematic,  $I_{IMU,acc}$  is the typical IMU supply current while operating as an accelerometer, and  $I_{IMU,gyr}$  is the typical IMU supply current while operating as a gyroscope. The worst-case scenario turned out not to introduce that much uncertainty since the current consumption by the embedded controller only differed by 12 mA. It is important to note that  $I_7$

is doubled due to both  $R_7$  and the other I<sup>2</sup>C pull-up resistor  $R_8$  being of the same value. A more detailed description of the embedded controller, IMU, and I<sup>2</sup>C content is discussed later.

Additionally, the current calculations for  $I_{HES}$ , as well as a more detailed description of the Hall effect sensors will be discussed later. Because  $I_{DD}$  turned out to be less than the rated current of the AP7381 regulator, the current consumption was deemed sufficient. This also meant that the minimum charge capacity of the selected LiPo cell had to be 308 mA·h, when discharging at 0.2C. To accommodate for both the regulator and the charge controller, that was when it was decided that a 500 mA·h battery would suffice. From Equation 3 for  $I_L = I_{DD}$ , the maximum power dissipation was calculated to be about 322 mW. The voltage regulator has thermal regulation, overvoltage, and overcurrent protection capabilities as well. For the heat sink, the maximum thermal resistance that the voltage regulator can handle, depending on the package, is between 125 °C/W and 167 °C/W.  $C_3 - C3$  in the schematic, is a filter capacitor tied between BT2 and ground so higher frequencies do not interfere with the regulator. It should be noted that regulator VSS pin is tied to ground. (BR)

The IMU subsystem consists entirely of the Bosch BMI088 inertial measurement unit – U6 in the schematic of Figure 8. In terms of hardware, the main concerns are power and communication. For power, the output of the voltage regulation subsystem will be used to provide the IMU with a stable 3.3 V power supply voltage. For the communication aspect, the main design parameters are the pull-up resistor values. Here, 10 k $\Omega$  resistors are used to limit current consumption while pulling the data and clock lines high when they need to be. (CM)

The embedded controller subsystem – U5 in Figure 8 – is the brain of the entire operation and will be realized with a PIC24FJ1024GB610 microcontroller. In the above schematic, most of the capacitors deal with voltage regulation and bypass. The other pins connect to other

subsystems: the SCL/SDA pins connect to the IMU subsystem, the interrupt pins connect to the Hall effect sensor subsystem, and the remaining two general purpose pins connect to the brake actuation subsystem. It is worth noting that the hardware interrupt pins are being pulled down by the Hall effect sensors, so the typical pullup/down resistors are not needed for those pins in this design. The last general purpose output pins will connect to NPN bases in the power dissipation network. Their purpose is to drive the logic behind which parts of the power dissipation network are operating and at what capacity. PWM, or pulse width modulation, on those pins is a way to have more fine-tuned control over the actuation on the MOSFETs rather than using them as simple switches. To program the microcontroller, it was decided that an ICD4 module, which is represented as the A-2004-1-LP-N-R modular connector J1 in Figure 8, would be used. Per the PIC24F datasheet, resistors  $R_9$  and  $R_{10}$  –  $R_9$  and  $R_{10}$  in the schematic – were incorporated as part of the external debugger circuitry and were set to be  $10\text{ k}\Omega$  and  $470\ \Omega$ , respectively.

Additionally, decoupling capacitors  $C_5$  and  $C_{13}$  –  $C_5$  and  $C_{13}$  in the schematic – were incorporated, and a value of  $100\text{ nF}$  for each capacitor was chosen. Per the PIC24F datasheet, decoupling capacitor  $C_6$  –  $C_6$  in the Figure 8, was included between the VCAP pin and ground to block high frequencies with the chip's internal voltage regulator, and that capacitance was set to  $10\ \mu\text{F}$ . and decoupling capacitors  $C_k$ , where  $k = 7, 8, \dots, 12$ . are connected between each VDD pin and VSS – ground – pin on the microcontroller. The values for  $C_k$  –  $C_k$  on Figure 8 – were chosen to be  $100\text{ nF}$ . For the subsystem demonstration, it should be note that an Explorer 16/32 Development Board was used to program the embedded controller instead of the ICD4 module.

(LM, CM)

For the Hall effect sensor subsystem, it was decided two AH3362Q Hall effect sensors, particularly AH3362Q-P-A devices would be used due to its fast response times, compactness

and lightness, and the fact that it is more easily mountable than a surface mount device. Additionally, all of the signal processing needed to create a digital logic signal is integrated into the device, making for a much simpler overall design. The AH3362Q devices, labeled as U3 and U4, have open-drain outputs that are pulled up to  $V_{reg}$  via 100 k $\Omega$  resistors and  $R_5$ , respectively – the high resistance is just to minimize current consumption. Those two resistors are also labeled in as R4 and R5, respectively. In terms of just a single device, the Hall effect sensor will switch and latch onto a logic low when a magnetic flux density of at least 3 mT is sensed by the device. When the magnetic flux density drops below 2 mT, the sensor will switch and latch to a logic high. The outputs of U3 and U4 will feed into the RD0 and RD10 pins of the microcontroller. The microcontroller is denoted as U5 on the schematic. The response time, according to the datasheet, is 3.75  $\mu$ s, which is fast enough for this application. Also, using the datasheets, the total current consumption by one Hall effect sensor  $I_{HES}$  was calculated to be between 3.03 and 4.03 mA – the supply current is between 3 mA and 4 mA, while the output current was calculated to 33  $\mu$ A using Equation 21, but replacing  $R_{2,3}$  with  $R_{4,5}$ . Using Equations 5 and 6, as well as graphical analysis, it was determined that at least one 9144 NdFeB disc magnet per wheel was adequate for measuring the wheel speed. C4 is a filter capacitor for the Hall effect sensors, and the value of 47 nF was recommended by the sensor datasheet. (BR)

With the energy dissipation system, an approach was taken to make the system resemble a dynamic braking system. To achieve the theoretical maximum power dissipation of 166.5 W, two 2.2  $\Omega$ , 100 W power resistors – R12 and R14 in the schematic – are connected in parallel. Two Yaegoo JK-0228 brushed DC motors – M1 and M2 in the schematic – will be used as generators. The chosen DC motor is rated for a maximum voltage of 24 V at 150 W. The 150 W from the motor would not meet the requirement, but market limitations and size between the two

motors when placed into the device were taken into consideration. With the inclusion of friction, the motors will be able to meet the requirements. Using brushed DC motors instead of a brushless system will make the output as a single-phase reducing hardware requirement. The TIP31C power transistors – Q3 and Q4 in Figure 8 – have a maximum voltage of 100 V, well below the maximum voltage generated from the generator. In experimentation for the subsystem demonstration, the response time was below the maximum 100 ms response time. (RH)

## 5.2. Software Design (LM, CM)

### 5.2.1. Level 0

The following figure shows a high-level overview of the inputs and outputs of the software.

The software is taking in data from this project’s makeshift tachometers and IMU data. (CM)

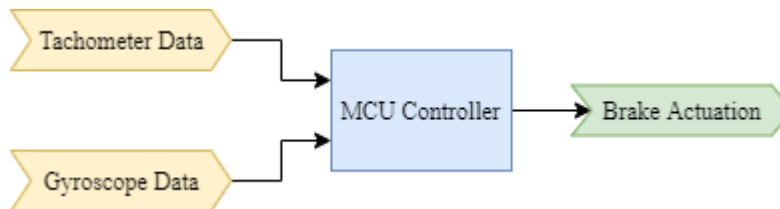


Figure 9: Level 0 Software Block Diagram

Table 6: Level 0 Software Functional Requirement Table

Module	MCU Controller
<b>Inputs</b>	<ul style="list-style-type: none"> <li>• Tachometer data</li> <li>• Gyroscope data</li> </ul>
<b>Outputs</b>	<ul style="list-style-type: none"> <li>• Brake Actuation</li> </ul>
<b>Description</b>	<ul style="list-style-type: none"> <li>• Automatically prevents longboard from exceeding predetermined speed limit and will keep the longboard at that speed until it drops below the limit (without slipping)</li> </ul>

### 5.2.2. Level 1

The following block diagram is a breakdown of the basic inputs, outputs, and internal software subsystems. The tachometer data are split into two separate wheels, which are used with the gyroscope data in the physics calculations. The physics calculations send information to the braking conditionals, which determine the braking status of the system. (CM)

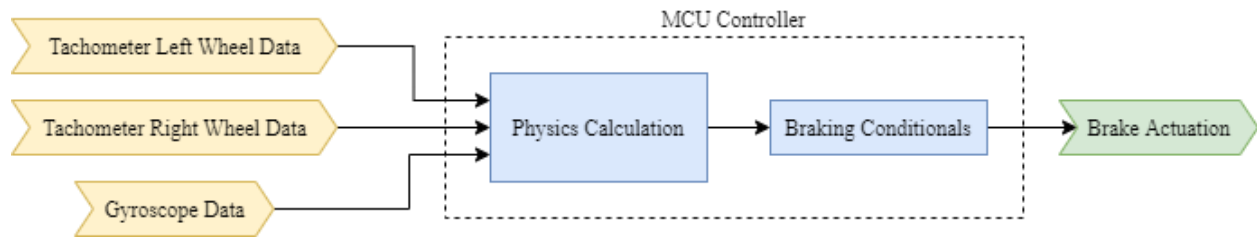


Figure 10: Level 1 Software Block Diagram

Table 7: Level 1 Software Function Requirement Tables

Module	Physics Calculation
Designer(s)	Corey Miller
Inputs	<ul style="list-style-type: none"> <li>Tachometer Left Wheel Data</li> <li>Tachometer Right Wheel Data</li> <li>Gyroscope Data</li> </ul>
Outputs	<ul style="list-style-type: none"> <li>Acceleration</li> <li>Linear Velocity</li> </ul>
Description	<ul style="list-style-type: none"> <li>Calculates the system's linear velocity by using the rotational velocity of the wheels</li> <li>Calculates the system's acceleration by using the current angle of descent</li> </ul>

Module	Braking Conditionals
Designer(s)	Logan Mashchak
Inputs	<ul style="list-style-type: none"> <li>Physics Calculation</li> </ul>
Outputs	<ul style="list-style-type: none"> <li>Brake State (Velocity braking, Acceleration Limiting, or no braking)</li> </ul>
Description	<ul style="list-style-type: none"> <li>Decides if engaging (or disengaging) brakes is necessary</li> </ul>



### 5.2.3. Level 2

The Level 2 Software block diagram is shown below in Figure 11. Here, the physics calculations are divided into two additional subsystems: velocity and acceleration calculations. Specifically, the velocity calculations are using the wheel rotational velocity data and converting it to linear velocity for usage in the conditionals. The acceleration calculation uses the gyroscope data and outputs the current linear acceleration of the system, assuming the system weighs 200 pounds. The braking conditionals are also further divided. At this level, the conditionals decide the braking state of the system: disengaging the brakes for slippage, engaging the brakes for velocity, and engaging the brakes to minimize the acceleration. (LM)

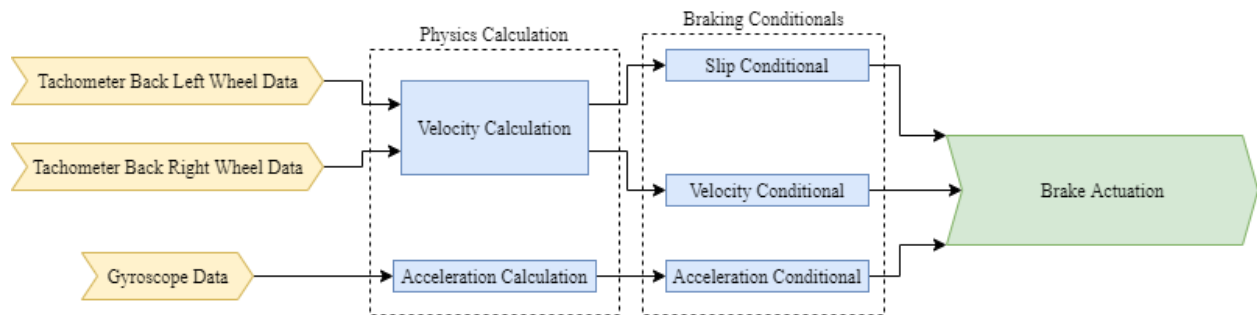


Figure 11: Level 2 Software Block Diagram

Table 8: Level 2 Software Functional Requirement Tables

Module	Velocity Calculation
Designer(s)	Corey Miller
Inputs	<ul style="list-style-type: none"> <li>Tachometer Back Left Wheel Data</li> <li>Tachometer Back Right Wheel Data</li> </ul>
Outputs	<ul style="list-style-type: none"> <li>Linear velocity</li> </ul>
Description	<ul style="list-style-type: none"> <li>Calculates the system's linear velocity by using the rotational velocity of the wheels</li> </ul>

<b>Module</b>	Acceleration Calculation
<b>Designer(s)</b>	Corey Miller
<b>Inputs</b>	<ul style="list-style-type: none"> <li>Gyroscope Data</li> </ul>
<b>Outputs</b>	<ul style="list-style-type: none"> <li>Linear acceleration</li> </ul>
<b>Description</b>	<ul style="list-style-type: none"> <li>Calculates the system's acceleration by using the current angle of descent</li> </ul>

<b>Module</b>	Slip Conditional
<b>Designer(s)</b>	Logan Mashchak
<b>Inputs</b>	<ul style="list-style-type: none"> <li>Velocity calculation result</li> </ul>
<b>Outputs</b>	<ul style="list-style-type: none"> <li>Returns a value that either skips the other conditionals due to slip detection or continues the conditionals if slip is not detected</li> </ul>
<b>Description</b>	<ul style="list-style-type: none"> <li>Checks to see if velocities of both wheels match. If they do not, then braking will be avoided in order to correct the found slip.</li> </ul>

<b>Module</b>	Velocity Conditional
<b>Designer(s)</b>	Logan Mashchak
<b>Inputs</b>	<ul style="list-style-type: none"> <li>Velocity calculation result</li> </ul>
<b>Outputs</b>	<ul style="list-style-type: none"> <li>Returns either velocity braking state to brake actuation or signals to check for acceleration conditional</li> </ul>
<b>Description</b>	<ul style="list-style-type: none"> <li>Checks if velocity is at threshold velocity (12 mph). If at threshold, braking will actuate accordingly. If below threshold, the program will continue to next conditional.</li> </ul>

<b>Module</b>	Acceleration Conditional
<b>Designer(s)</b>	Logan Mashchak
<b>Inputs</b>	<ul style="list-style-type: none"> <li>• Acceleration calculation result</li> </ul>
<b>Outputs</b>	<ul style="list-style-type: none"> <li>• Returns either acceleration limiting state to brake actuation or signals no braking needs to be done</li> </ul>
<b>Description</b>	<ul style="list-style-type: none"> <li>• Checks to see if acceleration is approaching acceleration threshold. If at threshold, the braking will actuate lightly to limit maximum acceleration. If below threshold, the program will release or not engage brakes.</li> </ul>

**5.2.4 Software Pseudocode, Flow Charts, and Formal Code (LM, CM)**

The implementation of the velocity calculation subsystem block is realized with the following algorithm. Firstly, the microcontroller boots and runs setup code. Such setup requires the initialization of four global variables along with the interfacing of two external hardware interrupts and one timer interrupt. Two global variables and one hardware interrupt correspond to each wheel. The timer interrupt is used for both wheels. As explained in the hardware discussion, the Hall effect sensors will be used to send a pulse signal to the controller, the frequency being directly proportional to the rotational velocity of the wheels. On each pulse, the external hardware interrupt is triggered. The interrupt service routine uses one of the global variables to count how many interrupts have occurred since initialization. Upon triggering the timer interrupt, the pulse counts from each wheel are moved into other global variables, one each. The values from these global variables are the ones being used in calculations. This design makes calculation significantly more deterministic because there is no need to calculate moving averages, account for variance in passed time between readings, or implement a mutual exclusion variable for reading from the count variable. Instead, the time between every pulse count update is always known and there is no possibility of race conditions occurring between

the external interrupts and other subsystems reading the value from the variable. The following pseudocode and flow chart in Figures 12 and 13, respectively, show this process being carried out, and formal code for the algorithm explained above is shown in Figure 14. (CM)

```
Setup External Interrupt Handlers

Declare leftTemp, leftCurrent, rightTemp, RightCurrent

On Left Interrupt:
  leftTemp++

On Right Interrupt:
  rightTemp++

On Timer Interrupt:
  set leftCurrent = leftTemp
  set leftTemp = 0

  set rightCurrent = rightTemp
  set rightTemp = 0
```

Figure 12: Velocity Calculation Pseudocode

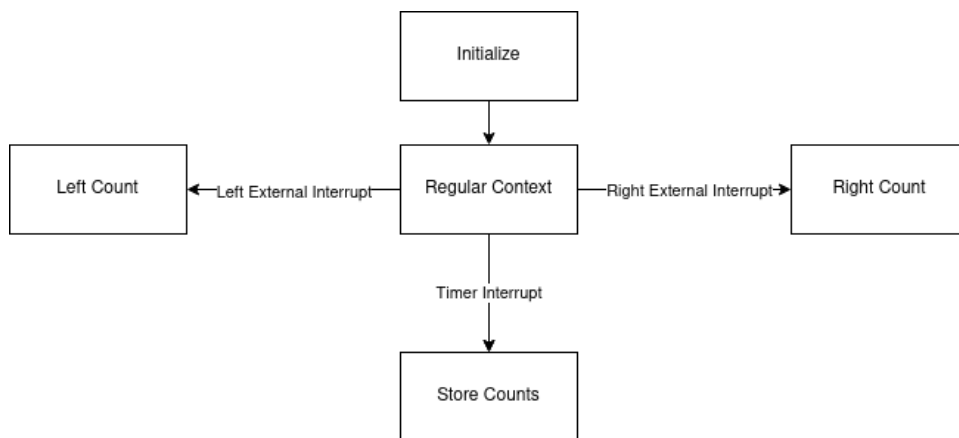


Figure 13: Velocity Calculation Flow Chart

```

void setup_timer_interrupt(void)
{
    _T1IP = 1;
    TMR1 = 0;
    PR1 = 16000 - 1;

    T1CON = 0x8030;
    _T1IF = 0;
    _T1IE = 1;
}

void _ISR_T1Interrupt(void)
{
    current_left_count = left_count;
    left_count = 0;

    _T1IF = 0;
}

void __attribute__((__interrupt__, no_auto_psv)) _INT0Interrupt(void)
{
    left_count = left_count + 1;

    IFS0bits.INT0IF = 0;
}

void setup_external_interrupts()
{
    TRISD = 0x01;
    INTCON2bits.INT0EP = 0;
    IEC0bits.INT0IE = 1;
    IPC0bits.INT0IP = 3;
    IFS0bits.INT0IF = 0;
    INTCON2bits.GIE = 1;
}

```

Figure 14: Formal Velocity Calculation Code

For the acceleration calculation, its implementation mainly concerns the stability of reading the variable upon which the board's acceleration is dependent: the angle of descent. This subsystem is centered around reading values from the inertial measurement unit (IMU), stabilizing them, then converting them to a single angle value to be used in the acceleration conditionals. Before taking readings from the IMU, the IMU needs to be powered on and configured. The focus of configuration is setting the resolution at which the accelerometer and gyroscope operate. For the accelerometer, the resolution was set to 5460 LSB/g, yielding an

operating range of 6g of acceleration in any direction on any axis. The gyroscope resolution was set to the highest resolution, which is 262.144 LSB/deg/s. The high resolution for the gyroscope is important because of the operational range of the skateboard outlined in the engineering requirements: the skateboard needs to operate within a range of 0 to 4 degrees. Since 4 degrees is a small angle, the sacrifice of the gyroscopic reading range is not significant when compared to the benefits of reading very slight changes in the angle of elevation. After initialization, the IMU is ready to provide readings to the system. At the beginning of every iteration, the accelerometer and gyroscope values are obtained. Next, the system needs to perform conversions. Selecting which variables are used in the conversions is a matter of choosing an axis upon which the IMU is rotating, then using the IMU values that correspond to that axis. For measuring the angle of elevation upon the y-axis, the accelerometer values on the x- and z-axes and the gyroscope value of the y-axis are used. Next, these values need to be converted to angles. For the accelerometer readings, the inverse tangent of the ratio of the x-axis to z-axis readings is taken. The *atan2* function from the C math library is used, though the output of that function needs to be converted from radians to degrees. The value from *atan2* is thus multiplied by 57.296 ( $180/\pi$ ) and then assigned to a variable charged with holding the angle obtained from the accelerometer. Next, the gyroscope reading is converted to an angle. As discussed in Section 2.3.2, this conversion is simply an integration of the rate obtained by the gyroscope that is added to the previously calculated gyroscope angle value. Lastly, the angle values of the gyroscope and accelerometer are passed through a complementary filter, which scales the gyroscope value to 98% and the accelerometer value to 2%, and the filter outputs are summed together. This technique effectively filters out the high variance of the accelerometer while mitigating the drift caused by repeated integration of the gyroscope values. The pseudocode and flow chart in Figures 15 and

16, respectively, illustrate this algorithm's implementation. Formal code scripts for reading the gyroscope and accelerometer values and for the complementary filter are shown in Figures 17, 18, and 19, respectively. (CM)

```
Set up I2C and power on IMU
Set IMU measurement resolution

set lastAngle = 0

do forever:
  read gyroscope
  read accelerometer

  set gyroAngle = gyroy * timeSinceLastRead + lastAngle
  set accelerometerAngle = arctangent( accelX / accelZ ) * 180/pi

  set currentAngle = 0.98*gyroAngle + 0.02*accelerometerAngle
  set lastAngle = currentAngle
```

Figure 15: Pseudocode of IMU Readings and Calculations

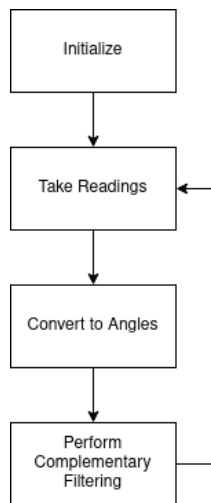


Figure 16: Flow Chart of IMU Readings

```

void Read_Gyroscope(void)
{
    char test[6];

    I2Cstart();
    I2Csendbyte(GYRO_ADDRESS_W);
    I2Csendbyte(GYRO_REG_DATA);
    I2Cstop();

    I2Cstart();
    I2Csendbyte(GYRO_ADDRESS_R);
    int i;
    for(i = 0; i < 5; i++)
    {
        test[i] = I2Cgetbyte(0);
    }

    test[5] = I2Cgetbyte(1);

    I2Cstop();

    gyrox = test[0] + test[1]*256;
    gyroy = test[2] + test[3]*256;
    gyroz = test[4] + test[5]*256;
}

```

Figure 17: Formal Code for Reading Gyroscope

```

void Read_Accelerometer(void)
{
    char test[6];

    I2Cstart();
    I2Csendbyte(ACC_ADDRESS_W);
    I2Csendbyte(ACC_REG_DATA);
    I2Cstop();

    I2Cstart();
    I2Csendbyte(ACC_ADDRESS_R);
    int i;
    for(i = 0; i < 5; i++)
    {
        test[i] = I2Cgetbyte(0);
    }

    test[5] = I2Cgetbyte(1);

    I2Cstop();

    accx = test[0] + (test[1]*256);
    accy = test[2] + (test[3]*256);
    accz = test[4] + (test[5]*256);
}

```

Figure 18: Formal Code for Reading Accelerometer



```

void Complementary_Filter(int dt)
{
    accangle = 57.296 * atan2(accz, accx);

    angle = 0.98 * ((double)gyroy * 0.0038 * dt / 1000 + prevAngle) +
    0.02 * accangle;

    prevAngle = angle;
}

```

Figure 19: Formal Complementary Filter Code

The braking decision/braking conditional process is broken down into 3 subroutines that decide when braking should occur: Slip check, Velocity check, and Acceleration check. The slip check is performed first, as it has the highest priority of all the conditionals. Slip check is conducted by first calculating the absolute error of the left and the right wheel and checking to see if the error is within the allowable 5% error margin. If it is above the margin, the “predictor” value, a value that is the velocity of the previous cycle added to the current acceleration times dt, will be used to determine which wheel is slipping or skidding. Whichever wheel speed is farther apart from the predicted value will be recognized as the slipping wheel. The velocity of the non-slipping wheel is also noted for the predictor of the next cycle. This wheel will be noted so it can be disengaged. The velocity conditional, second in priority, is then performed. This is conducted by checking if the *faster* of the two wheels has approached the limit of 12 miles per hour. If so, both wheels will be noted so that braking protocol activates for both, unless one was detected slipping earlier. The faster velocity is also noted for the predictor of the next cycle. The acceleration conditional, final in priority, is then performed. This is conducted by checking to see if the acceleration has approached the limit of 0.65 m/s<sup>2</sup>. If so, both wheels will be noted so that acceleration braking protocol activates for both, unless one was detected slipping earlier. The faster velocity is also noted for the predictor of the next cycle. The pseudocode and flow chart

demonstrating the braking conditional algorithm can be seen in Figures 20 and 21, respectively, and formal code for the algorithm can be seen in Figure 22. (LM)

```
//velocityLeft and velocityRight are the velocity values grabbed from measured values for each wheel
//velocityNext is a predictor value used to determine what the velocity should be this iteration
//accel is the accel value grabbed from measured angle value from IMU
//leftBrakeDecision and rightBrakeDecision are decider states to return as the final decision. they
will have 4 states: indecisive, engage, disable, and damper (damper is used for accel braking)
//deciderVelocity is used as a placeholder for an ACCURATE velocity value after slip detection
finishes
step 1)
  set velocityLeft = velocityLeftMeasured
  set velocityRight = velocityRightMeasured
  set accel = accelMeasured
  set velocityNext = deciderVelocityPrevious + accel*.100
  set leftBrakeDecision = indecisiveBit
  set rightBrakeDecision = indecisiveBit
step 2)
  is velocityLeft similar to velocityRight?
    if YES, deciderVelocity == velocityLeft && goto step 4
    if NO, goto step 3
step 3)
  is abs(velocityLeft - velocityNext) > abs(velocityRight - velocityNext)?
    if YES, leftBrakeDecision = disableBit && deciderVelocity = velocityRight && goto step 4
    if NO, rightBrakeDecision = disableBit && deciderVelocity = velocityLeft && goto step 4
step 4)
  is deciderVelocity > 12 MPH?
    if YES, goto step 5
    if NO, goto step 6
step 5)
  if (leftBrakeDecision == indecisiveBit)
    then leftBrakeDecision = engageBit
  if (rightBrakeDecision == indecisiveBit)
    then rightBrakeDecision = engageBit
  goto step 9
step 6)
  is accel > .65 m/s^2?
    if YES, goto step 7
    if NO, goto step 8
step 7)
  if (leftBrakeDecision == indecisiveBit)
    then leftBrakeDecision = damperBit
  if (rightBrakeDecision == indecisiveBit)
    then rightBrakeDecision = damperBit
  goto step 9
step 8)
  leftBrakeDecision = disableBit
  rightBrakeDecision = disableBit
  goto step 9
step 9)
  return leftBrakeDecision && rightBrakeDecision
```

Figure 20: Pseudocode for Braking Conditionals

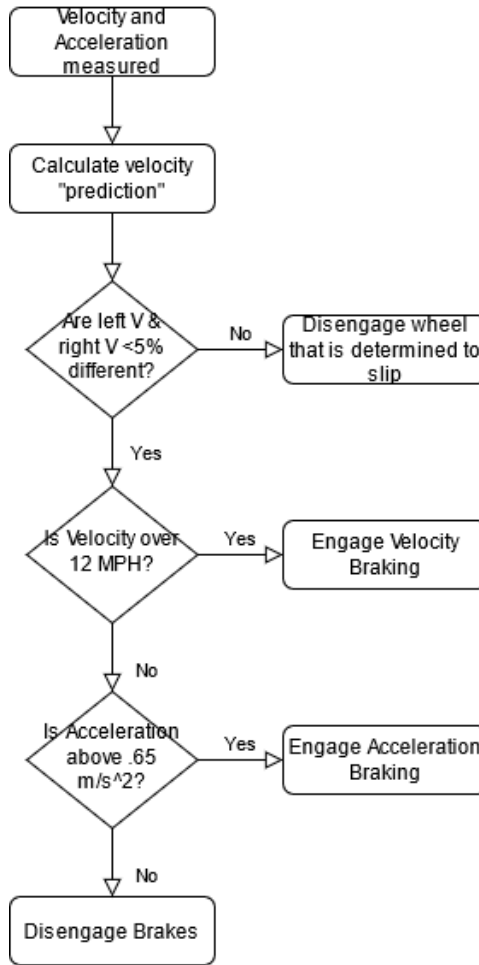


Figure 21: Flow Chart for Braking Conditionals

```

static int leftSuperBool = 0; // global variable -- 0 is indecisive, 1 is disable, 2 is
engage, 3 is damper
static int rightSuperBool = 0; // global variable -- 0 is indecisive, 1 is disable, 2
is engage, 3 is damper
static int speed_prev;

void brake(float vLeft, float vRight, float accel)
{
    float abs = vLeft / vRight;
    float avg = (vLeft + vRight)/2;
    float lDev, rDev, vDecider;
    float vPredict = speed_prev + accel*.1;
    vDecider = vLeft;
    if(vRight > vLeft)
    {
        vDecider = vRight;
    }
    if(abs <= .95 || abs >= 1.05)
    {
        lDev = fabs(vLeft - speed_prev);
        rDev = fabs(vRight - speed_prev);
        if(rDev > lDev){
            rightSuperBool = 1;
            vDecider = vLeft;
        } else {
            leftSuperBool = 1;
            vDecider = vRight;
        }
    }
    if (vDecider > 12) {
        speed_prev = avg;
        if(leftSuperBool != 1)
            leftSuperBool = 2;
        if(rightSuperBool != 1)
            rightSuperBool = 2;
    } else if (accel > .65) {
        speed_prev = avg;
        if(leftSuperBool != 1)
            leftSuperBool = 3;
        if(rightSuperBool != 1)
            rightSuperBool = 3;
    } else {
        speed_prev = avg;
        leftSuperBool = 1;
        rightSuperBool = 1;
    }
} //the "super bools" are then used for braking decision

```

Figure 22: Formal Braking Conditionals Code

## 6. Mechanical Sketch (LM)

Figure 23 below shows a mechanical sketch of the longboard anti-lock braking system previously discussed. The rectangular box towards the center of the board represent the electronic circuitry (except for the Hall effect sensors), and the mechanical components, which include the motors, support and gear mechanisms, and the Hall effect sensors, can be seen to the left of the rectangular box.

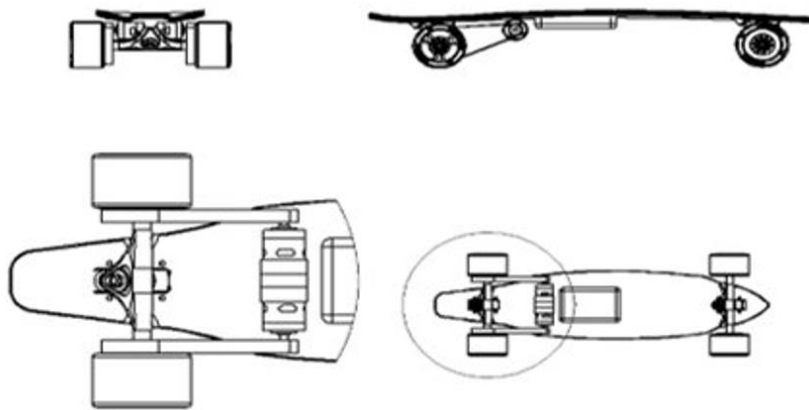


Figure 23: Longboard Control System Mechanical Sketch

## 7. Team Information (RH)

Raymond Hoyle, Electrical Engineering

Logan Mashchak, Computer Engineering

Corey Miller, Computer Engineering

Ben Roter, Electrical Engineering

## 8. Part List (RH, LM, CM, BR)

### 8.1 Parts List

Figure 24 shows the list of parts used for this design.

1	Qty.	Refdes	Part Num.	Description
2				
3	1		BMI088	EVAL BOARD FOR BMI088
4	2	Q1	BS170	MOSFET N-CH 60V 500MA TO-92
5	2	Q2	BS250P	MOSFET P-CH 45V 230MA E-LINE
6	2		IPC0067	DFN-10 TO DIP-14 SMT ADAPTER
7	2	Q3,Q4	TIP31C	TIP31C NPN power transistor
8	2	SW1	CST10T2CR	Toggle Switch
9	2	R12,R14	HS100 2R2 J	2.2 Ohms ±5% 100W Wirewound Chassis Mount Resistor
10	2	BT1		3.7V Lithium Polymer Battery Rechargeable (Secondary) 500mAh
11	1			FISH SKATEBOARDS 41-Inch Downhill Longboard
12	2			Vanpro DIY Electric Skateboard 5065 Brushless Motor Mount Bracket 80MM
13	1			Cloud Ride! Longboard Wheels Hurricanes 90mm 78A (Set of 4) Blue
14	2	M1, M2		Yaegoo 150W 24V DC Electric Motor Brushed Motor Fit
15	6	U1	MCP73213T-A6X/MF	Charger IC Lithium Ion/Polymer 10-DFN (3x3)
16	1		8195	Magnet Neodymium Iron Boron (NdFeB) N35 0.250" Dia x 0.063" H (6.35mm x 1.59mm)
17	1		9144	N52 MAGNET DISK D1/4X1/4" 1=20PC
18	2	U2	AP7381-33V-A	Linear Voltage Regulator IC Output 150mA TO-92
19	2	U2	L4931CZ33-AP	Linear Voltage Regulator IC Output 250mA TO-92-3
20	2	U3	AH3362Q-P-A	Digital Switch Unipolar Switch Open Drain Hall Effect 3-SIP
21	2	U3	SI7201-B-11-IBR	Digital Switch Omnipolar Switch Open Drain Hall Effect TO-92-3
22	2	U3	AH1806-P-A	Digital Switch Omnipolar Switch Open Drain Hall Effect 3-SIP
23	1	U6	LSM9DS1TR	IMU ACCEL/GYRO/MAG I2C/SPI 24LGA
24	2	R11, R13		1k Ohms 1/4 W resistor
25	1	U5		Pic24FJ1024GB610
26	7	C5, C7, C8, C9, C10, C11, C12		100 nF ceramic capacitor
27	3	R7, R8, R9		10k Ohms 1/4 W resistor
28	1	R10		470 Ohms 1/4 W resistor
29	1	C6		10 uF 50 V ceramic capacitor
30	3	R1, R4, R5		100k Ohms 1/4 W resistor
31	1	C4		47 nF ceramic capacitor
32	3	C1, C2, C3		1 uF ceramic capacitor
33	2	R2, R3		340 Ohms 1/4 W resistor
34	1	R_prog		5.16k Ohms 1/4 W resistor

Figure 24: Parts List

## 8.2. Material Budget List

Figure 25 shows the budget list that contains expenditures for the design currently.

2	Qty.	Part Num.	Description	Unit Cost	Total Cost
3					
4	1	BMI088	EVAL BOARD FOR BMI088	25.00	25.00
5	2	BS170	MOSFET N-CH 60V 500MA TO-92	0.45	0.90
6	2	BS250P	MOSFET P-CH 45V 230MA E-LINE	0.83	1.66
7	2	IPC0067	DFN-10 TO DIP-14 SMT ADAPTER	5.79	11.58
8	2	TIP31C	TIP31C NPN power transistor	0.57	1.14
9	2	CST10T2CR	Toggle Switch	2.64	5.28
10	2	HS100 2R2 J	2.2 Ohms $\pm$ 5% 100W Wirewound Chassis Mount Resistor	11.07	22.14
11	2		3.7V Lithium Polymer Battery Rechargeable (Secondary) 500mAh	6.95	13.90
12	1		FISH SKATEBOARDS 41-Inch Downhill Longboard	59.49	59.49
13	2		Vanpro DIY Electric Skateboard 5065 Brushless Motor Mount Br	38.00	76.00
14	1		Cloud Ride! Longboard Wheels Hurricanes 90mm 78A (Set of 4) E	62.95	62.95
15	2	JK-0228	Yaegoo 150W 24V DC Electric Motor Brushed Motor Fit	30.99	61.98
16	6	MCP73213T-A6X/MF	Charger IC Lithium Ion/Polymer 10-DFN (3x3)	1.79	10.74
17	1	8195	Magnet Neodymium Iron Boron (NdFeB) N35 0.250" Dia x 0.063"	0.23	0.23
18	1	9144	N52 MAGNET DISK D1/4X1/4" 1=20PC	11.99	11.99
19	2	AP7381-33V-A	Linear Voltage Regulator IC Output 150mA TO-92	0.44	0.88
20	2	L4931CZ33-AP	Linear Voltage Regulator IC Output 250mA TO-92-3	0.65	1.30
21	2	AH3362Q-P-A	Digital Switch Unipolar Switch Open Drain Hall Effect 3-SIP	0.97	1.94
22	2	SI7201-B-11-IBR	Digital Switch Omnipolar Switch Open Drain Hall Effect TO-92-3	0.70	1.40
23	2	AH1806-P-A	Digital Switch Omnipolar Switch Open Drain Hall Effect 3-SIP	0.76	1.52
24	1	LSM9DS1TR	IMU ACCEL/GYRO/MAG I2C/SPI 24LGA	6.14	6.14
25	2		1k Ohms 1/4 W resistor		
26	1		Pic24FJ1024GB610		
27	7		100 nF ceramic capacitor		
28	3		10k Ohms 1/4 W resistor		
29	1		470 Ohms 1/4 W resistor		
30	1		10 uF 50 V ceramic capacitor		
31	3		100k Ohms 1/4 W resistor		
32	1		47 nF ceramic capacitor		
33	3		1 uF ceramic capacitor		
34	2		340 Ohms 1/4 W resistor		
35	1		5.16k Ohms 1/4 W resistor		
36					
37					
38					
39				<b>Total</b>	<b>\$378.16</b>

Figure 25: Material Budget List

## 9. Project Schedules (RH, LM, CM, BR)

Figures 26 and 27 show the Gantt charts created to help schedule different parts of the project.

Task Mode(C/I)	Task Name	Duration	Start	Finish	Predecessor
	SDP   2020	98	8/26/2020	12/2/2020	
C	<b>Project design</b>	40	8/26/2020	10/5/2020	
C	<b>Midterm Report</b>	21	9/14/2020	10/5/2020	
C	Cover page	0	9/14/2020	9/14/2020	
C	T of C, L of T, L of F	20	9/14/2020	10/4/2020	
C	<b>Problem Statement</b>	21	9/14/2020	10/5/2020	
C	Need	0	9/14/2020	9/14/2020	
C	Objective	0	9/14/2020	9/14/2020	
C	Background	0	9/14/2020	9/14/2020	
C	Marketing Requirements	7	9/14/2020	9/21/2020	
C	Engineering Requirement Specification	21	9/14/2020	10/5/2020	
C	<b>Engineering Analysis</b>	14	9/14/2020	9/28/2020	
C	Circuit (DC,AC,Power,...)	14	9/14/2020	9/28/2020	
C	Electronics (analog and digital)	14	9/14/2020	9/28/2020	
C	Signal Processing	14	9/14/2020	9/28/2020	
C	Communications (analog and digital)	14	9/14/2020	9/28/2020	
C	Electromechanics	14	9/14/2020	9/28/2020	
C	Computer Networks	14	9/14/2020	9/28/2020	
C	Embedded Systems	14	9/14/2020	9/28/2020	
C	<b>Accepted Technical Design: Phase 1</b>	21	9/14/2020	10/5/2020	
C	<b>Hardware Design: Phase 1</b>	2	9/14/2020	9/16/2020	
C	Hardware Block Diagrams Level 0 thru N (w/	2	9/14/2020	9/16/2020	
C	<b>Software Design: Phase 1</b>	15	9/14/2020	9/29/2020	
C	Software Behavior Models 0 thru N (w/ FR ta	15	9/14/2020	9/29/2020	
C	<b>Mechanical Sketch</b>	21	9/14/2020	10/5/2020	
C	<b>Team information</b>	0	9/14/2020	9/14/2020	
C	<b>Project Schedules</b>	15	9/14/2020	9/29/2020	
C	Midterm Design Gantt Chart	15	9/14/2020	9/29/2020	
C	<b>References</b>	21	9/14/2020	10/5/2020	
C	<b>Midterm Parts Request Form</b>	40	8/26/2020	10/5/2020	
C	Midterm Design Presentation Day 1	0	9/30/2020	9/30/2020	
C	Midterm Design Presentation Day 2	0	10/7/2020	10/7/2020	
C	<b>Project Poster</b>	14	11/18/2020	12/2/2020	
I	<b>Final Design Report</b>	50	10/6/2020	11/25/2020	
I	Abstract	48	10/6/2020	11/23/2020	
I	Hardware Design: Phase 2	48	10/6/2020	11/23/2020	
I	Modules 1...n	48	10/6/2020	11/23/2020	
I	Simulations	48	10/6/2020	11/23/2020	
I	Schematics	48	10/6/2020	11/23/2020	
I	Software Design: Phase 2	48	10/6/2020	11/23/2020	
I	Modules 1...n	48	10/6/2020	11/23/2020	
I	Code (working subsystem)	48	10/6/2020	11/23/2020	
I	System integration Behavior Models	48	10/6/2020	11/23/2020	
I	Parts Lists	48	10/6/2020	11/23/2020	
I	Parts list(s) for schematics	48	10/6/2020	11/23/2020	
I	Material Budgets list	48	10/6/2020	11/23/2020	
I	Proposed implementation Gantt Chart	48	10/6/2020	11/23/2020	
I	Conclusion and Recommendations	48	10/6/2020	11/23/2020	
I	<b>Final Parts request Form</b>	13	10/11/2020	10/24/2020	
I	Subsystem Demonstration Day 1	0	11/10/2020	11/10/2020	
I	Subsystem Demonstration Day 2	0	11/17/2020	11/17/2020	

Figure 26: Midterm Gantt Chart



35		✦	<b>Project Poster</b>	16 days	Wed 11/18/20	Fri 12/4/20	
36		✦	<b>Final Design Report</b>	50 days	Tue 10/6/20	Wed 11/25/20	
37		✦	<b>Abstract</b>	48 days	Tue 10/6/20	Mon 11/23/20	
38		✦	▾ <b>Hardware Design: Phase 2</b>	<b>52 days</b>	<b>Fri 10/2/20</b>	<b>Mon 11/23/20</b>	
39		✦	▾ <b>Modules 1...n</b>	<b>52 days</b>	<b>Fri 10/2/20</b>	<b>Mon 11/23/20</b>	
40		✦	Simulations	48 days	Tue 10/6/20	Mon 11/23/20	
41		✦	Raymond Hoyle	38 days	Wed 10/7/20	Sat 11/14/20	
42		✦	Corey Miller	38 days	Fri 10/2/20	Mon 11/9/20	
43		✦	Benjamin Roter	38 days	Tue 10/6/20	Fri 11/13/20	
44		✦	<b>Schematics</b>	48 days	Tue 10/6/20	Mon 11/23/20	
45		✦	Raymond Hoyle	38 days	Wed 10/7/20	Sat 11/14/20	
46		✦	Corey Miller	38 days	Fri 10/2/20	Mon 11/9/20	
47		✦	Benjamin Roter	38 days	Tue 10/6/20	Fri 11/13/20	
48		✦	▾ <b>Software Design: Phase 2</b>	<b>91 days?</b>	<b>Mon 8/24/20</b>	<b>Mon 11/23/20</b>	
49		✦	▾ <b>Modules 1...n</b>	<b>91 days?</b>	<b>Mon 8/24/20</b>	<b>Mon 11/23/20</b>	
50		✦	Code (working subsystems)	48 days	Tue 10/6/20	Mon 11/23/20	
51		✦	Slip	38 days	Tue 10/6/20	Fri 11/13/20	
52		✦	Velocity	32 days	Tue 10/6/20	Sat 11/7/20	
53		✦	Acceleration	36 days	Tue 10/6/20	Wed 11/11/20	
54		✦	<b>System integration Behavior Models</b>	48 days	Tue 10/6/20	Mon 11/23/20	
55		✦	Slip	28 days	Fri 10/16/20	Fri 11/13/20	
56		✦	Velocity	32 days	Tue 10/6/20	Sat 11/7/20	
57		✦	▾ <b>Parts Lists</b>	<b>48 days</b>	<b>Tue 10/6/20</b>	<b>Mon 11/23/20</b>	
58		✦	Parts list(s) for Schematics	48 days	Tue 10/6/20	Mon 11/23/20	
59		✦	Materials Budget list	48 days	Tue 10/6/20	Mon 11/23/20	
60		✦	<b>Proposed Implementation Gantt Chart</b>	48 days	Tue 10/6/20	Mon 11/23/20	
61		✦	<b>Conclusions and Recommendations</b>	48 days	Tue 10/6/20	Mon 11/23/20	
62		✦	Final Parts Request Form	13 days	Sun 10/11/20	Sat 10/24/20	
63		✦	Subsystems Demonstrations Day 1	6.38 days	Tue 11/10/20	Mon 11/16/20	
64		✦	Subsystems Demonstrations Day 2	1 day	Mon 11/16/20	Tue 11/17/20	
65		✦	Parts Request Form for Spring Semester	9 days	Mon 11/23/20	Wed 12/2/20	

Figure 27: Final Gantt chart

## 10. Conclusions and Recommendations (RH, LM, CM, BR)

When developing the automatic longboard anti-lock braking system, there were many parts of the design process that were successful – choosing suitable devices for measuring and monitor wheel speed and longboard angle, choosing a suitable power source and charging method, choosing a suitable microcontroller and suitable algorithms for controlling braking in different situations, and choosing a suitable method for removing energy from the longboard system. There are still various issues that need to be mitigated in the future with respect to hardware – both electrical/electronic and mechanical – and software because of the design choices previously made.

(BR)

With respect to mechanical hardware, the regenerative braking method was preferred over the caliper style braking because of constraints with the wheels. Caliper style braking would significantly degrade the plastic of the wheels and implementing the design would be considerably difficult- the time spent on designing the mechanics of the caliper design could be better spent on thinking about the electronics. Nevertheless, mounting the mechanical parts and interfacing them with the electrical and electronic hardware will need a careful approach. (RH)

The main issues being faced currently from an electrical perspective are battery power consumption for the embedded controller and logic circuitry, charging the batteries, how power coming from the regenerative motors should be dissipated, how to minimize the component sizes and amounts to conserve space underneath the longboard. For the battery pack, testing needs to be done to more accurately determine both how long it takes the two batteries to fully charge from being “dead” and how long it takes them to discharge assuming the worst-case current consumption. Additionally, sensing distances for the longboard vis-à-vis the Hall effect sensors and their magnets are a concern due to the physical limitations around the wheel-axle connections underneath the longboard. In terms of braking, a circuit topology that changes the output impedance of the regenerative motors is of concern – a varying amount of power needs to be dissipated in the circuit as heat, and the inductive properties of the motors also need to be mitigated somehow in the design. To get around the spatial limitations of underneath the longboard for the electronic components, it was decided that a printed circuit board will be designed so that connections and component and device sizes can be better controlled. (RH, BR)

In terms of software, there are still issues that need be considered with respect to response, computation, and performance times. Further testing needs to be done to ensure that the physics calculations are within the response and performance time stipulations set in the engineering

requirements discussed before, as the computation time increases as calculations become more numerous and/or more complicated. Making sure that the output data from the complementary filter is as clean as possible while accounting for computing time and computing power is of great importance still when it comes time for the braking conditionals to start. Lastly, further testing needs to be done from an integration standpoint so that the mechanical and electrical hardware interface with the software in a complete manner. (LM, CM)

## 11. References (RH, LM, CM, RH)

Erjavec, Jack. "47." *Automotive Technology: A Systems Approach*. N.p.: Delmar/Thomson Learning, 2004. 1201-213. Print.

"Brakeboard Pty Ltd." *Brakeboard*, Brakeboard, [www.brakeboard.com/pages/home](http://www.brakeboard.com/pages/home).

llingworth, Cynthia, et al. "Skateboard Injuries: Preliminary Report." *The B Medical Journal*, vol. 2, no. 6103, 1977, pp. 1636–1636. JSTOR.

Koch-Dücker, Heinz-Jürgen, and Ulrich Papert. "Antilock Braking System (ABS)." *Brakes, Brake Control and Driver Assistance Systems*, Springer Fachmedien Wiesbaden, 2014, pp. 74–75.

Kumar, Deepak, et al. "A Review Paper on Anti-Lock Braking System (ABS) and Advancement." *International Journal of Management, Technology And Engineering*, International Journal of Management, Technology And Engineering, May 2018, [www.ijamtes.org/gallery/2.%20m.e%20-%2002.pdf](http://www.ijamtes.org/gallery/2.%20m.e%20-%2002.pdf).

McKenzie, Lara B., et al. "Epidemiology of Skateboarding-Related Injuries Sustained by Children and Adolescents 5-19 Years of Age and Treated in US Emergency Departments: 1990 through 2008." *Injury Epidemiology*, BioMed Central, 8 Apr. 2016, [inpejournal.biomedcentral.com/articles/10.1186/s40621-016-0075-6](http://inpejournal.biomedcentral.com/articles/10.1186/s40621-016-0075-6)

"Mellow: The Electric Drive That Fits under Any Skateboard – Mellow Boards GmbH." *The Electric Skateboard Drive That Fits under Any Skateboard*, [www.mellowboards.com/en/FAQ/](http://www.mellowboards.com/en/FAQ/).

Miller, Mike, et al. "Requirements Analysis Document." *Michigan State University College of Engineering*, Michigan State University, 19 Oct. 2001,

[www.cse.msu.edu/~cse470/F01/Projects/ABS/ABS3/web/ReqAnalysis/Rev1/requirements.pdf](http://www.cse.msu.edu/~cse470/F01/Projects/ABS/ABS3/web/ReqAnalysis/Rev1/requirements.pdf).

Pang, Yik Hang. *Electrical Transportation Tool*. Patent 838,793 S1. 22 Jan. 2019.

Peles, Zalman. *Antilock and Antiskid Mechanical Brake System for Vehicles and Method Thereof*. Patent 7,299,901. 27 Nov. 2007.

Pretagostini, Francesco et al. "Anti-Lock Braking Control Design Using a Nonlinear Model Predictive Approach and Wheel Information." 2019 IEEE International Conference on Mechatronics (ICM) 1 (2019): 525-530.

"Regenerative Braking and Conserving Battery Charge." *Boosted*, [support.boostedboards.com/hc/en-us/articles/115000912488-Regenerative-Braking-and-Conserving-Battery-Charge](http://support.boostedboards.com/hc/en-us/articles/115000912488-Regenerative-Braking-and-Conserving-Battery-Charge).

Sheu, Yahtyng, et al. "Sports- and Recreation-Related Injury Episodes in the United States, 2011–2014." *National Health Statistics Reports*, Center for Disease Control and Prevention, 18 Nov. 2016, [www.cdc.gov/nchs/data/nhsr/nhsr099.pdf](http://www.cdc.gov/nchs/data/nhsr/nhsr099.pdf).

"DIY Electric Skateboard Kit & Parts - Build A DIY Electric Skateboard." *DIY Electric Skateboard*, 28 Sept. 2020, [diyelectricskateboard.com/](http://diyelectricskateboard.com/).

"BU-107: Comparison Table of Secondary Batteries." *Secondary (Rechargeable) Batteries – Battery University*, [batteryuniversity.com/learn/article/secondary\\_batteries](http://batteryuniversity.com/learn/article/secondary_batteries).

"Detailed Anti-Slip Tape Info." *Safety Direct America*, 17 Sept. 2018, [safetydirectamerica.com/anti-slip-tapes/anti-slip-tape-additional-info-and-test-data/](http://safetydirectamerica.com/anti-slip-tapes/anti-slip-tape-additional-info-and-test-data/).

sdm\_admin, Posted by. "The Magnetic Field Strength of Permanent Magnet." *SDM Magnetics Co.,Ltd*, 7 Aug. 2020, [www.magnet-sdm.com/2017/08/01/magnetic-field-strength-permanent-magnet/](http://www.magnet-sdm.com/2017/08/01/magnetic-field-strength-permanent-magnet/).

## 12. Datasheets (RH, LM, CM, BR)

LSM9DS1: [www.st.com/en/mems-and-sensors/lsm9ds1.html](http://www.st.com/en/mems-and-sensors/lsm9ds1.html)

TIP31C: <https://www.onsemi.com/pdf/datasheet/tip31c-d.pdf>

AH3362Q-P-A: <https://www.diodes.com/assets/Datasheets/AH3362Q.pdf>

PIC24FJ1024GB610:

<https://ww1.microchip.com/downloads/en/DeviceDoc/PIC24FJ1024GA610-GB610-Family-Data-Sheet-DS30010074G.pdf>

AH1806: <https://www.diodes.com/assets/Datasheets/AH1806.pdf>

BMI088: <https://www.bosch-sensortec.com/media/boschsensortec/downloads/datasheets/bst-bmi088-ds001.pdf>

AP7381-33V-A: <https://www.diodes.com/assets/Datasheets/AP7381.pdf>

ASR00035:

[https://media.digikey.com/pdf/Data%20Sheets/TinyCircuits%20PDFs/ASR00035\\_Web.pdf](https://media.digikey.com/pdf/Data%20Sheets/TinyCircuits%20PDFs/ASR00035_Web.pdf)

MCP73213-A6X/MF: <https://ww1.microchip.com/downloads/en/devicedoc/20002190c.pdf>

SLI-343P8G3F:

[https://d1d2qsbl8m0m72.cloudfront.net/en/products/databook/datasheet/opto/led/lamp\\_mono/sli-343x8-e.pdf](https://d1d2qsbl8m0m72.cloudfront.net/en/products/databook/datasheet/opto/led/lamp_mono/sli-343x8-e.pdf)

WP5603SIDL/SD/J3: <https://www.kingbrightusa.com/images/catalog/SPEC/WP5603SIDL-SD-J3.pdf>

CST10T2CR: <https://www.citrelay.com/Catalog%20Pages/SwitchCatalog/CST.pdf>

JK-0228: <https://www.amazon.com/Yaegoo-Electric-Brushed-Scooter-Experiment/dp/B07MQKCB7F>

A-2004-1-4-LP-N-R: <https://datasheet.octopart.com/A-2004-1-4-LP-N-R-Assmann-Electronics-datasheet-66132448.pdf>